Transportation Research Part C 129 (2021) 103182

Contents lists available at ScienceDirect

Transportation Research Part C

journal homepage: www.elsevier.com/locate/trc

Lane-change-aware connected automated vehicle trajectory optimization at a signalized intersection with multi-lane roads

Handong Yao, Xiaopeng Li *

Department of Civil and Environmental Engineering, University of South Florida, 4202 E Fowler Avenue, ENC 3300, Tampa, FL 33620, United States

A R T I C L E I N F O

Keywords:
Mixed traffic
Connected automated vehicle
Decentralized control
Trajectory smoothing
Lane-change-aware
Signalized intersections

A B S T R A C T

Trajectory smoothing is an effective concept to control connected automated vehicles (CAVs) in mixed traffic to reduce traffic oscillations and improve overall traffic performance. However, smoother trajectories often lead to greater gaps between vehicles, which may incentivize human driven vehicles (HVs) from adjacent lanes to make cut-in lane changes. Such cut-in lane changes may compromise the expected performance from CAV trajectory smoothing. To figure out the reasons behind the issue, this paper designs a mixed traffic framework at a signalized intersection with multi-lane roads considering detailed trajectory control, car following and lane changing maneuvers all together. Based on the framework, this paper proposes a decentralized lane-change-aware CAV trajectory optimization model including discretionary lane change restraining and mandatory lane change yielding strategies. Riding comfort and traffic mobility are considered as a joint objective. And the complex non-linear lane-change-aware constraints are linearized to convert the proposed problem to a quadratic optimization problem. The linearization allows the investigated problem to be easily fed into a commercial solver. Numerical experiments are conducted to study the performance of the proposed model and to compare it with other models (e.g., a cooperative lane change model and a trajectory optimization model without the lane-change-aware mechanism) in different scenarios. First, results show that the HV lane changes cause reduction of half or more expected benefits of trajectory smoothing along a multi-lane segment adjacent to a signalized intersection. Then, we find that the proposed model outperforms the other models. Especially, the proposed model yields extra benefits in the system joint objective (10–25%), riding comfort (10–25%), travel time (1–8%), fuel consumption (3–15%) and safety (5–25%) compared with the trajectory optimization model without the lane-change-aware mechanism when CAV market penetration rate is not high. Sensitivity analyses on road segment lengths, signal cycle lengths, traffic saturation rates and through-vehicle rates show that the proposed model yields better system performance under most scenarios, e.g., 20% extra benefit at a short road segment length, 30% extra benefit at a long signal cycle length, 25% extra benefit at a high traffic saturation rate, and 25% extra benefit at a high through-vehicle rate.

1. Introduction

The United States Department of Transportation (USDOT) emphasized the crucial role of connected automated vehicle (CAV) technologies that enable information sharing among individual automated (or autonomous) vehicles to increase safety, efficiency, and

* Corresponding author.
E-mail address: xiaopengli@usf.edu (X. Li).

https://doi.org/10.1016/j.trc.2021.103182
Received 14 October 2020; Received in revised form 20 April 2021; Accepted 26 April 2021
Available online 4 June 2021
0968-090X/Published by Elsevier Ltd.

reliability of the transportation system (USDOT, 2018). Trajectory smoothing is an effective concept to reduce traffic oscillation and has been widely used with the idea of avoiding sharp acceleration/deceleration by optimizing speed profiles. Various methods, such as eco-driving, Green Light Optimal Speed Advisory, Cooperative Adaptive Cruise Control, shooting heuristic algorithm and dynamic programming, are proposed to implement trajectory smoothing for energy efficiency, as well as mobility and safety. The detailed review of CAV trajectory optimization methods could be found in Wang et al. (2018).

Due to different automation technologies among CAVs, the Society of Automotive Engineers (SAE) defined levels of automation (SAE, 2020) as follows: 1) Level 0: no driving automation; 2) Level 1: driver assistance; 3) Level 2: partial driving automation; 4) Level 3: conditional driving automation; 5) Level 4: high driving automation; 6) Level 5: fully driving automation. In the near future with the interaction of human drivers (e.g., Level 0 - Level 2), eco-driving will be used to smooth trajectories because of its capability to be implemented with the interaction of human drivers. With the improvement of CAV technologies in a bit more distant future (e.g., Level 3 - Level 5), trajectory smoothing will be used to yield system-level optimization performance. Therefore, we consider CAVs with Level 3+ of automation technologies in this paper.

Further, due to different communications and cooperation behavior among CAVs, the SAE defined classes of cooperation (SAE, 2020) as follows: 1) Class A: Status sharing. CAVs have full authority to decide actions based on the perception information about the traffic environment and the status of participants, such as current locations and speeds of vehicles, and current signal phase; 2) Class B: Intent sharing. CAVs have full authority to decide actions based on the information about the planned future actions of participants, such as planned trajectories and departure times of vehicles, and signal phase and timing (SPaT); 3) Class C: Agreement seeking. CAVs have full authority to decide actions with a sequence of collaborative messages among specific CAVs intended to influence local planning of related actions; 4) Class D: Prescriptive. CAVs have full authority to decide actions except for very specific circumstances in which they are designed to accept and adhere to a prescriptive communication.

In this paper, we focus on a mixed traffic environment where CAVs are considered as in cooperation class B or above (per the SAE J3216 standard) and the data of human driven vehicles (HVs) are shared by vehicle-to-everything (V2X) communication technologies (e.g., dedicated short range communication [DSRC] systems) or collected as proxy connected vehicle data by road-side detectors (e.g., loop-detectors, cameras, lidars, and radars). Thus, CAVs and HVs can share their status (e.g., locations and speeds) and intents (e.g., estimated departure times) with other participants (e.g., road side units, traffic lights, CAVs and HVs), and CAVs can decide their actions based on the information about the planned future actions of participants. The state-of-art studies in such mixed traffic environment have shown that the interactions between CAVs and HVs affect traffic performance in mobility, fuel efficiency and safety via car following behavior and lane changing behavior.

In single-lane mixed traffic, only car following behavior exists. CAVs are capable of communicating with surroundings (e.g., vehicles and infrastructures) and precisely control their speeds to improve roadway capacity and fuel efficiency on highway without experiencing lane change (LC) impacts (Aria et al., 2016; Chen et al., 2017; Liu et al., 2018; Ghiasi et al., 2019; Chen et al., 2020). Studies have proved that CAV trajectory smoothing has the potential to reduce travel time/delay and fuel consumption, and to enhance riding comfort and safety by releasing traffic oscillations with smooth trajectories at intersections with a single-lane road (Treiber et al., 2014; Ma et al., 2017; Taylor and Zhou, 2017; Wei et al., 2017; Slade et al., 2020). These benefits are found out to increase with growing CAV market penetration rates (MPRs) in mixed traffic (He and Wu, 2018; Jiang et al., 2017; Wan et al., 2016; Yang et al., 2017; Yao and Li, 2020; Zhao et al., 2018; Pourmehrab et al., 2020a; Pourmehrab et al., 2020b).

In multi-lane mixed traffic, both car following behavior and lane changing behavior exist. A number of models and strategies have been proposed to investigate CAV LC related policies and strategies, such as CAV lane assignment (Bevly et al., 2016; Chen et al., 2017; Ghiasi et al., 2019) and CAV lane changing control (You et al., 2015; Wang et al., 2015; Bevly et al., 2016; Yu et al., 2018). In this paper, only HV LCs are considered because all CAVs are assumed to follow the planned trajectories and will not conduct LCs. Ioannou et al. (2005) demonstrated that a high probability of HV cut-in LCs from adjacent lanes exists due to the large gaps created by adaptive cruise control deceleration behavior. Besides, Milanés and Shladover (2016) demonstrated that HV cut-in LCs drastically increase traffic oscillation in cooperative adaptive cruise control systems equipped platoons. To handle HV cut-in LCs on freeways, efforts have been made on two aspects: HV cut-in LC detection (Kazemi et al., 2018; Muslim and Itoh, 2018; Choi and Gi, 2019) and CAV control coping with HV cut-in LCs (Ko and Chang, 2018; Zhang et al., 2018; Chen et al., 2020). These CAV control strategies will regulate CAVs' speeds to yield larger gaps for HVs to cut in. Although these CAV control strategies could maximize travel efficiency, safety, and riding comfort on freeways, they might cause negative effects at signalized intersections. Since traffic signals would interrupt vehicles and cause full stops, trajectory smoothing is adopted to help vehicles pass an intersection with less full stops. With larger gaps generated by trajectory smoothing at a signalized intersection, the probability of HV cut-in LCs is supposed to be higher. To date, only a few studies have investigated the effects of HV cut-in LCs on CAV trajectory smoothing at a signalized intersection with a brief description of lane changing maneuvers (Xia et al., 2013; Kamal et al., 2015; Wan et al., 2016; Yang et al., 2017). Xia et al. (2013) found that fuel/emission benefits from trajectory smoothing at a signalized intersection are weakened since HVs have more flexibility to change lanes with larger gaps. Yang et al. (2017) concluded that trajectory smoothing at signalized intersections has negative impacts on overall system performance due to the LCs around the controlled CAVs when the CAV MPR is low. While the existing studies confirmed the negative impacts of HV cut-in LCs on the system performance of trajectory smoothing in mixed traffic using simulators, they focused on the longitudinal maneuvers (e.g., longitudinal control and car following) but the lateral maneuver (e.g., lane changing) was only described with a few sentences. Therefore, there is no such mixed traffic framework that connects trajectory control, car following and lane changing maneuvers all together at a signalized intersection with multi-lane roads. Further, none of them investigate the trigger of the HV cut-in LCs let alone propose mechanisms to restrain the HV LCs induced by trajectory smoothing at a signalized intersection. If we use the same freeway CAV yielding strategy at a signalized intersection, a CAV has to yield a larger gap to let an HV cut-in. Thus, the CAV will not follow the planned trajectory and the negative impacts (e.g., extra oscillation, delay and

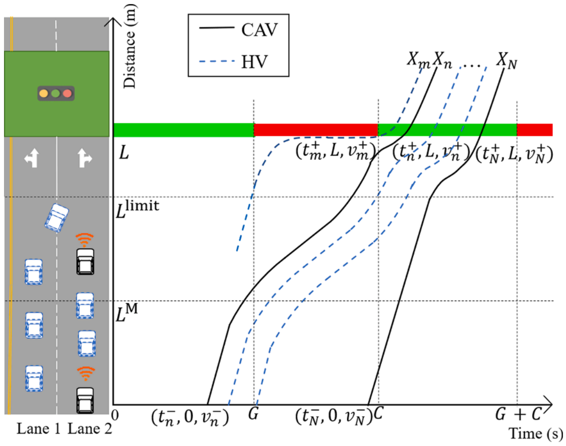

Fig. 1. An illustration of the CAV trajectory optimization at a signalized intersection with a two-lane road.

energy consumption) will not be addressed.

Motivated by the above research gaps, this paper designs a mixed traffic framework at a signalized intersection with multi-lane roads, including a trajectory planning module that is running on CAVs and a trajectory control module with car following and lane changing maneuvers that is running on both CAVs and HVs. Then, this paper proposes a decentralized lane-change-aware CAV trajectory optimization model (LCTO) under the framework to address the HV LCs induced by trajectory smoothing with mandatory LC yielding and discretionary LC restraining strategies. A joint objective is considered with riding comfort and mobility. Nonlinear LC-aware constraints, considering both discretionary LCs and mandatory LCs, are linearized for modeling LCTO into a quadratic optimization problem. A set of numerical experiments are then conducted to verify the effectiveness of LCTO and to compare it with a trajectory optimization model (TO) without the lane-change-aware mechanism and a cooperative lane change model (i.e., TO with a LC yielding strategy [LCTOY]). First, we find that the expected benefits of trajectory smoothing are overestimated without considering LCs, and the actual benefits in TO with LCs are decreased half or more compared with the expected benefits without LCs. Then, sensitivity analysis results on CAV market penetration at a signalized intersection with multi-lane roads show that LCTO is better than the other models. Especially, LCTO yields significant extra benefits in the system joint objective (10–25%), riding comfort (10–25%), safety (5–25%), travel time (1–8%) and fuel consumption (3–15%) when the CAV MPR is not high. Other sensitivity analysis results on road segment lengths, signal cycle lengths, traffic saturation rates and through-vehicle rates show that TO is recommended with the same system performance as LCTO but higher computational efficiency when either the road segment length is relatively long or the through-vehicle rate is relatively low, and LCTO is suggested in other traffic scenarios with significant extra benefits in the system joint objective (e.g., at most 20%, 30%, 25% and 25% extra benefits regarding road segment lengths, signal cycle lengths, traffic saturation rates and through-vehicle rates, respectively).

The contributions of this paper include the following aspects.

1) This paper designs a mixed traffic framework at a signalized intersection with multi-lane roads considering trajectory control, car following, lane changing maneuvers all together to investigate the reasons behind the HV LCs induced by trajectory smoothing.
2) This paper proposes a decentralized lane-change-aware CAV trajectory optimization model with mandatory LC yielding and discretionary LC restraining strategies in mixed traffic at a signalized intersection with multi-lane roads.
3) CAV market penetration analyses are conducted to verify that the expected benefits of trajectory smoothing are impaired by HV LCs, and LCTO is capable of improving the system riding comfort, travel time, fuel consumption and safety when the CAV MPR is not high.
4) Sensitivity analyses on road segment lengths, signal cycle lengths, traffic saturation rates and through-vehicle rates imply that LCTO is effective in most traffic situations except those when the road segment length is too long and the through-vehicle rate is too low.

The organization of this paper is as follows. Section 2 describes the mixed traffic framework at a signalized intersection with multi-lane roads. Section 3 formulates LCTO with discretionary LC restraining and mandatory LC yielding strategies. Section 4 conducts numerical experiments to study the performance of LCTO under different traffic settings. Section 5 discusses the limitations and extensions of LCTO. Finally, Section 6 concludes this manuscript and briefly discusses future research directions.

2. Extension of the existing trajectory optimization model in a multi-lane context

This section describes the mixed traffic framework at a signalized intersection with multi-lane roads. The focus of this framework is on a signalized intersection with a fixed-time signal setting, formed by a two-lane road (note that the two-lane setting is for conciseness of the presentation and it can be easily adapted to multi-lane instances, see Appendix D), as illustrated by Fig. 1. For convenience of readers, the key notation is listed in Appendix A.

Consider a time horizon of $\mathcal{T} := [0, T]$, where T is the time window for CAV trajectory control. Consider a two-lane road segment approaching a signalized intersection with a control zone of length L. Let L^{limit} denote the location after which LCs are prohibited. Let L^{M} denote the location after which mandatory LCs are activated. Let $\mathcal{K} := [1, K]$ denote the set of lanes, where K is the number of lanes. Let $k = 1$ denote the leftmost lane (i.e., lane 1), and the index increases rightwards, thus indicating $k = K$ as the rightmost lane (i.e., lane K). Note that $K = 2$ in the two-lane setting.

Let $\mathcal{N} := 1, 2, \ldots, N$ denote the set of vehicles. $\mathcal{N}^{\text{HV}} := 1, 2, \ldots, N^{\text{HV}}$ and $\mathcal{N}^{\text{CAV}} := N^{\text{HV}}+1, N^{\text{HV}}+2, \ldots, N^{\text{HV}}+N^{\text{CAV}} = N$ denote the sets of HVs (i.e., the blue-dashed curves in Fig. 1) and CAVs (i.e., the black-solid curves in Fig. 1), respectively. N^{HV} and N^{CAV} are the numbers of HVs and CAVs, respectively. Let $X_n = \{x_n(t)\}_{t\in\mathcal{T}}$ denote the trajectory of vehicle $n \in \mathcal{N}$, where $x_n(t)$ is the location of vehicle n at time t. Let $v_n(t) = \dot{x}_n(t) \in [0, \overline{v}]$, where $\overline{v}$ denotes the speed limit. And let $a_n\left(t\right) = \ddot{x}_n\left(t\right) \in \left[\underline{a}, \overline{a}\right]$ denote the acceleration of vehicle n, where $\underline{a}$ and $\overline{a}$ denote the minimum and maximum acceleration rates respectively.

Let e_n denote the desired turning movement of vehicle n, where $e_n = 0$ for through vehicles, $e_n = 1$ for left-turn vehicles, and $e_n = 2$ for right-turn vehicles. Assign lane 1 to through and left-turn vehicles and lane 2 to through and right-turn vehicles. Thus, the desired lane set $\widetilde{O}_n(e_n)$ of vehicle n is formulated as follows,

$$\widetilde{O}_n(e_n) = \begin{cases} \{1,2\}, & \text{if } e_n = 0; \\ \{1\}, & \text{if } e_n = 1; \\ \{2\}, & \text{otherwise.} \end{cases} \tag{1}$$

Assume the control zone is reserved for smoothing longitudinal CAV trajectories while CAV lateral LCs, if any, are completed upstream before arriving the control zone. Whereas HVs are randomly distributed in all lanes. Thus, in the control zone, CAVs will not make LCs, and only HVs will make LCs.

Additionally, let $o_n(t)$ denote the current lane of vehicle n at time t. In the two-lane setting, at time $t \in \mathcal{T}$, if a vehicle is located in lane 1, then its target lane (the lane to which vehicle n intends to change to) is lane 2. Otherwise, its target lane is lane 1. Thus, the target lane $o^*_n(t)$ of vehicle n at time t can be calculated as

$$o^*_n\left(t\right) = \begin{cases} o_n(t) + 1, & \text{if } o_n(t) = 1, \\ o_n(t) - 1, & \text{if } o_n(t) = 2. \end{cases} \tag{2}$$

Further, assume the intersection signal control follows a fixed signal timing plan with an effective green time G and an effective red time R, i.e., with a signal cycle length of $C = G+R$ (note that the yellow time is split and included in G and R). Assume that the intersection is equipped with road side units that allow the SPaT information to be shared with all connected vehicles in the control zone.

Let t^-_n and v^-_n denote the arrival time and arrival speed of vehicle n respectively, which are predetermined by the upstream traffic. To capture general stochastic vehicle arrival patterns with different traffic saturation rates (f^s) and green/cycle ratios (G/C), assume the arrival time of vehicle $n \in \mathcal{N}\backslash\mathcal{N}'$ follows the formulation in Ma et al. (2017).

$$t^-_n = \begin{cases} t^-_{l^-_n} + \left(\tau^{\text{CAV}} + \dfrac{s_0^{\text{CAV}} + l^{\text{veh}}}{v^-_n}\right) \times \left(1 + \xi_n \times \left(\dfrac{C}{f^s G} - 1\right)\right), & \text{if } n \in \mathcal{N}^{\text{CAV}}, \\ t^-_{l^-_n} + \left(\tau^{\text{HV}} + \dfrac{s_0^{\text{HV}} + l^{\text{veh}}}{v^-_n}\right) \times \left(1 + \xi_n \times \left(\dfrac{C}{f^s G} - 1\right)\right), & \text{otherwise,} \end{cases} \tag{3}$$

where ξ_n is an uniform random number over $[0, 2]$ and $f^s \in (0, C/G]$ is the traffic saturation rate. l^-_n is the initial preceding vehicle of vehicle n. τ^{CAV} and s_0^{CAV} are the minimum time gap and minimum spacing of a CAV, respectively. τ^{HV} and s_0^{HV} are the minimum time gap and minimum spacing of an HV, respectively. l^{veh} is the uniform vehicle length of a vehicle for all CAVs and HVs. Thus, $\tau^{\text{CAV}} + \frac{s_0^{\text{CAV}} + l^{\text{veh}}}{v^-_n}$ and $\tau^{\text{HV}} + \frac{s_0^{\text{HV}} + l^{\text{veh}}}{v^-_n}$ are the safety time gaps that ensure CAVs and HVs arrive without any collision. Additionally, $\mathcal{N}'$ is the set of leading vehicles (e.g., vehicles that do not have preceding vehicles) and the arrival time $t^-_{l^-_n \in \mathcal{N}'}$ of a leading vehicle is randomly selected. Each time, the arrival speed of vehicle n follows an uniform random number over $[\overline{v}/2, \overline{v}]$ to allow stochasticity in arrival speeds.

If vehicle n violates the safety spacing, the arrival times and speeds are changed to keep safety in the following ways. If $s_{n,l^-_n}(t^-_n) < s_0^{\text{CAV}} + \tau^{\text{CAV}} v^-_n, \forall n \in \mathcal{N}^{\text{CAV}}\backslash\mathcal{N}'$, we update

$$v^-_n = v^-_{l^-_n}, t^-_n = t^-_{l^-_n} + \tau^{\text{CAV}} + \frac{s_0^{\text{CAV}} + l^{\text{veh}}}{v^-_n}; \tag{4}$$

if $s_{n,l^-_n}(t^-_n) < s_0^{\text{HV}} + l^{\text{veh}} + \tau^{\text{HV}} v^-_n, \forall n \in \mathcal{N}^{\text{HV}}\backslash\mathcal{N}'$, we update

$$v^-_n = v^-_{l^-_n}, t^-_n = t^-_{l^-_n} + \tau^{\text{HV}} + \frac{s_0^{\text{HV}} + l^{\text{veh}}}{v^-_n}, \tag{5}$$

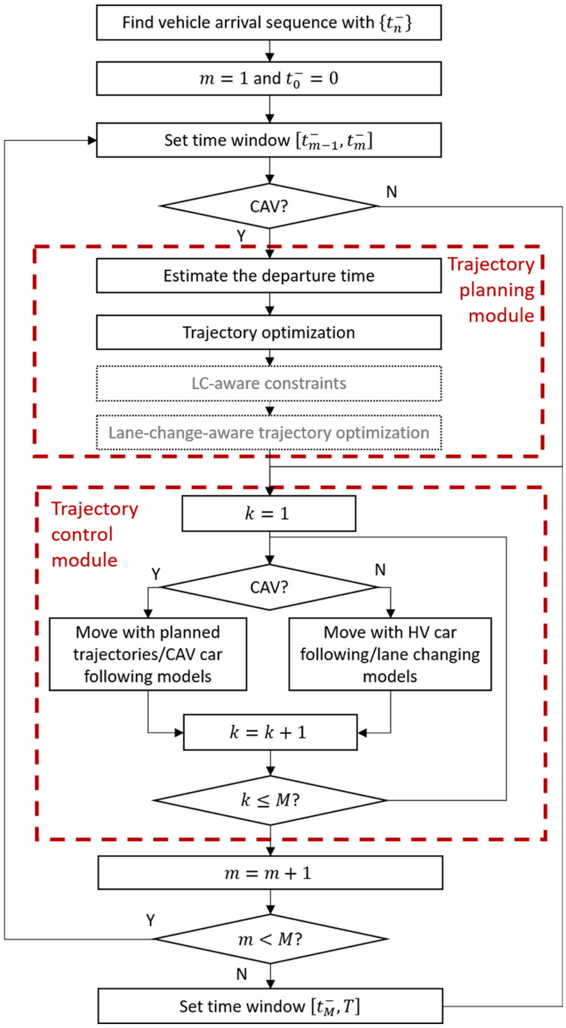

Fig. 2. Flow chart of the mixed traffic framework at a signalized intersection with multi-lane roads.

where $s_{n,m}(t) = x_m(t) - x_n(t) - l^{\text{veh}}$ is the spacing gap between vehicles n and m at time $t \in \mathcal{T}$.

Fig. 2 plots the flow chart of the mixed traffic framework at a signalized intersection with multi-lane roads. First, we check the arrival times of all vehicles to decide their arrival sequence. Then, a trajectory planning module is designed to optimize CAV trajectories within a rolling-time window. Note that the gray parts considering the LC-aware constraints are specific for LCTO and will not be used in TO. Last, a real-time trajectory control module is used to run on both CAVs and HVs at each time window. The detailed operations of these two modules are described in the following subsections.

2.1. Trajectory planning module

A decentralized control-based CAV trajectory optimization model (TO) has been studied in our previous work (Yao and Li, 2020) considering a signalized intersection with a single-lane road, and it can be extended to TO at a signalized intersection with multi-lane roads without considering possible conflicting HV LCs in a similar decentralized control scheme to reduce travel time and to improve riding comfort simultaneously. Thus, the continuous TO in the trajectory planning module is formulated as N^{CAV} sub-problems with each CAV as an individual sub-problem. For each CAV $n \in \mathcal{N}^{\text{CAV}}$,

$$\text{CTO}: \min_{X_n} J_n(X_n) := \omega_m \left(t_n^+ - t_n^-\right) + \omega_a \int_{t_n^-}^{\overline{t_n^+}} a_n(t)^2 dt, \tag{6}$$

where t_n^+ is the departure time of vehicle n. ω_m and ω_a are the weights of mobility and squared acceleration, respectively. Then, the continuous TO is subject to the following constraints.

- Arrival constraints:

$$x_n\left(t_n^-\right) = 0. \tag{7}$$

$$v_n\left(t_n^-\right) = v_n^-. \tag{8}$$

- Departure constraints:

$$x_n\left(t_n^+\right) = L. \tag{9}$$

$$\underline{t_n^+} \leqslant t_n^+ \leqslant \overline{t_n^+}, \tag{10}$$

where the lower bound of departure time $\underline{t_n^+}$ can be calculated by

$$\underline{t_n^+} = \mathcal{G}\left(\max\left\{t_n^- + \frac{\left(\overline{v} - v_n^-\right)^2}{2\overline{a}\overline{v}} + \frac{L}{\overline{v}}, t_{l_n(t_n^-)}^+ + \tau^{\mathrm{CAV}} + \frac{s_0^{\mathrm{CAV}} + l^{\mathrm{veh}}}{\overline{v}}\right\}\right). \tag{11}$$

$$\mathcal{G}\left(t\right) := \begin{cases} t, & \text{if } \operatorname{mod}(t, C) \in [0, G], \\ \lceil \frac{t}{C} \rceil \times C, & \text{otherwise.} \end{cases} \tag{12}$$

When vehicle n arrives at time t_n^-, the preceding vehicle $l_n(t_n^-)$ at time t_n^- is considered as the vehicle n's preceding vehicle until vehicle n departs. To let Eq. (11) satisfy leading vehicles, let $t_{l_{n'}(t_n^-)}^+ = -\infty, \forall n' \in \mathcal{N}'$. With Eq. (11), $\underline{t_n^+} = t_n^- + \frac{\left(\overline{v} - v_n^-\right)^2}{2\overline{a}\overline{v}} + \frac{L}{\overline{v}}$ if the trajectory of the preceding vehicle does not affect the subject vehicle. Otherwise, vehicle n should keep a safety spacing to the preceding vehicle, and thus $\underline{t_n^+} = t_{l_n(t_n^-)}^+ + \tau^{\mathrm{CAV}} + \frac{s_0^{\mathrm{CAV}} + l^{\mathrm{veh}}}{\overline{v}}$. With Eq. (12), the lower bound of departure time is definitely in green time.

To maintain a reasonable throughput, the upper bound of departure time $\overline{t_n^+}$ is set as

$$\overline{t_n^+} = \min\left\{\lfloor \frac{\underline{t_n^+}}{C} \rfloor \times C + G, \underline{t_n^+} + \tau^{\mathrm{CAV}} + \frac{s_0^{\mathrm{CAV}} + l^{\mathrm{veh}}}{\overline{v}}\right\}. \tag{13}$$

- Speed constraints:

$$0 \leqslant v_n(t) \leqslant \overline{v}, \ \forall t \in \left[t_n^-, \overline{t_n^+}\right]. \tag{14}$$

- Acceleration constraints:

$$\underline{a} \leqslant a_n(t) \leqslant \overline{a}, \ \forall t \in \left[t_n^-, \overline{t_n^+}\right]. \tag{15}$$

- Safety constraints:

$$x_{l_n(t_n^-)}\left(t\right) - x_n(t) \geqslant s_0^{\mathrm{CAV}} + l^{\mathrm{veh}} + \tau^{\mathrm{CAV}} v_n\left(t\right), \ \forall t \in \left[t_n^-, \overline{t_n^+}\right]. \tag{16}$$

Because $v_{l_{n'}(t)} = \overline{v}$ and $x_{l_{n'}(t)} = +\infty, \forall n' \in \mathcal{N}' \cap \mathcal{N}^{\mathrm{CAV}}$, Eq. (16) is also valid for leading CAVs. Eq. (16) is set to ensure safety between vehicle n and its preceding vehicle.

Although we can easily solve the continuous TO by commercial solvers (e.g., Gurobi) and smooth trajectory for each CAV, the planned trajectories are optimized based on the TO considering a single-lane road. At a signalized intersection with multi-lane roads, CAVs might not follow the planned trajectories due to HV LCs. Thus, the following trajectory control module is activated to control vehicles maintaining safety in real-time.

2.2. Trajectory control module

The trajectory control module is run on each vehicle to control vehicle's trajectory. If an HV arrives, the trajectory planning module will not work and the HV will follow predefined HV car following and lane changing models. If a CAV arrives, it will follow the planned trajectory and, if necessary, regulate its trajectory with a safety feature.

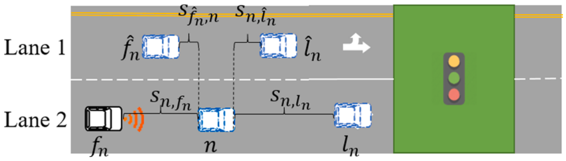

Fig. 3. An illustration of the HV lane changing model.

(1) HV car following model

HVs (i.e., $n \in \mathcal{N}^{\mathrm{HV}}$) follow Gipps' car following model described in Treiber and Kesting (2013).

$$v_n\left(t+\tau^{\mathrm{HV}}\right)=\begin{cases} F^{\mathrm{Gipps}}_{n,l_n(t)}\left(v_n(t), v_{l_n(t)}(t), s_{n,l_n(t)}(t)\right), & \\ \qquad\qquad \text{if } \operatorname{mod}(t, C)\in[0,G], & \\ \min\left\{F^{\mathrm{Gipps}}_{n,l_n(t)}\left(v_n(t), v_{l_n(t)}(t), s_{n,l_n(t)}(t)\right), F^{\mathrm{Gipps}}_{n,l_n(t)}\left(v_n(t),0,L+s_0^{\mathrm{HV}}-x_n(t)\right)\right\}, & \\ \qquad\qquad \text{otherwise.} & \end{cases} \tag{17}$$

$$F^{\mathrm{Gipps}}_{n,l_n(t)}\left(v_n(t), v_{l_n(t)}(t), s_{n,l_n(t)}(t)\right)=\min\left\{v_n(t)+\bar{a}\tau^{\mathrm{HV}}, \bar{v}, v^{\mathrm{safe}}_{HV}\left(v_{l_n(t)}(t), s_{n,l_n(t)}(t)\right)\right\}, \tag{18}$$

where $v^{\mathrm{safe}}_{HV}\left(v_{l_n(t)}(t), s_{n,l_n(t)}(t)\right)=\underline{a}\tau^{\mathrm{HV}}+\sqrt{\left(\underline{a}\tau^{\mathrm{HV}}\right)^2+v_{l_n(t)}(t)^2+2\underline{a}\times\left(s_{n,l_n(t)}(t)-s_0^{\mathrm{HV}}\right)}$ is the safe speed of an HV. Further, set $v_{l_n(t)}=\bar{v}$ and $x_{l_n(t)}=+\infty, \forall n' \in \mathcal{N}'$ to make Eq. (18) compatible with a leading vehicle. Note that we only consider the deterministic car following model in this paper to decrease the complexity of the stochastic behaviors and to focus on investigating the performance of the proposed lane-change-aware mechanism. The preliminary results of stochastic car following behavior can be found in Appendix E.

(2) HV lane changing model

The HV lane changing model is described in Treiber and Kesting (2013) involving safety and incentive checks. The safety checks require two components: safety check 1 with respect to the preceding vehicle on the target lane (Eq. (19)) and safety check 2 with respect to the following vehicle on the target lane (Eq. (20)).

$$s_{n,\widehat{l}_n(t)}\left(t\right)>s_0^{\mathrm{HV}}+\tau^{\mathrm{HV}}v_n\left(t\right)+\max\left\{0,\frac{v_{\widehat{l}_n(t)}(t)^2-v_n(t)^2}{2\underline{a}}\right\}, \tag{19}$$

$$\begin{cases} s_{\widehat{f}_n(t),n}\left(t\right)>s_0^{\mathrm{HV}}+\tau^{\mathrm{HV}}v_{\widehat{f}_n(t)}\left(t\right)+\max\left\{0,\dfrac{v_n(t)^2-v_{\widehat{f}_n(t)}(t)^2}{2\underline{a}}\right\}, \text{if } \widehat{f}_n\left(t\right)\in\mathcal{N}^{HV}, \\ s_{\widehat{f}_n(t),n}\left(t\right)>s_0^{\mathrm{CAV}}+\tau^{\mathrm{CAV}}v_{\widehat{f}_n(t)}\left(t\right)+\max\left\{0,\dfrac{v_n(t)^2-v_{\widehat{f}_n}\left(t\right)(t)^2}{2\underline{a}}\right\}, \text{otherwise.} \end{cases} \tag{20}$$

As shown in Fig. 3, $\widehat{f}_n(t)$ is the nearest following vehicle of vehicle n in the target lane at time t. To make Eq. (20) compatible to the last vehicle in a traffic stream, let $v_{\widehat{f}_N(t)}=0$ and $x_{\widehat{f}_N(t)}=-\infty$. Safety check 1 (i.e., Eq. (19)) passes when the spacing gap between vehicles n and $\widehat{l}_n(t)$ is greater than the safety spacing, and safety check 2 (i.e., Eq. (20)) passes when the spacing gap between vehicles n and $\widehat{f}_n(t)$ is greater than the safety spacing.

The incentive check is formulated as

$$\widetilde{a}_{n,\widehat{l}_n(t)}\left(t\right)-\widetilde{a}_{n,l_n(t)}\left(t\right)>\Delta a_n(t), \tag{21}$$

where $\widehat{l}_n(t)$ is the preceding vehicle of vehicle n in the target lane at time $t, \widetilde{a}_{n,l_n(t)}(t)=F^{\mathrm{Gipps}}_{n,l_n(t)}(\cdot)$ is the acceleration of vehicle n following its current preceding vehicle $l_n(t)$. And $\widetilde{a}_{n,\widehat{l}_n(t)}(t)=F^{\mathrm{Gipps}}_{n,\widehat{l}_n(t)}(\cdot)$ is the acceleration of vehicle n following its target preceding vehicle $\widehat{l}_n(t)$. Incentive check passes when $\widetilde{a}_{n,\widehat{l}_n(t)}(t)$ is great than $\widetilde{a}_{n,l_n(t)}(t)$ by a changing threshold of $\Delta a_n(t)$ at time t. This makes sure that an HV changes its lane only when there exists a significant mobility advantage, i.e., the increases of acceleration after the LC greater than $\Delta a_n(t)$.

Then, we consider two types of LCs: 1) discretionary LCs that are optional for a vehicle to improve its mobility and is not on the critical path for the vehicle to reach its destination, and 2) mandatory LCs that are required for a vehicle to reach its desired destination (i.e., $\widetilde{O}_n$). A conditional changing threshold $\Delta a_n(t)$ is used to represent these two types of LCs.

Before entering L^{M}, i.e., $x_n(t) \in [0, L^{\mathrm{M}})$, only the discretionary LCs are considered and $\Delta a_n(t) = 0.1$ according to Treiber and Kesting (2013). The discretionary LCs will occur when both safety and incentive checks pass. Between the locations L^{M} and L^{limit}, i.e., $x_n(t) \in [L^{\mathrm{M}}, L^{\mathrm{limit}})$, $\Delta a_n(t)$ is formulated as follows,

$$\Delta a_n(t) = \begin{cases} +\infty, \quad \text{if } o_n(t) \in \widetilde{O}_n \text{ and } o_n^*(t) \notin \widetilde{O}_n, -\infty, \text{if } o_n(t) \notin \widetilde{O}_n \text{ and } o_n^*(t) \in \widetilde{O}_n, 0.1, \text{otherwise.} \end{cases} \tag{22}$$

When the current lane is in the desired lane set and the target lane is not in the desired lane set (i.e., $\Delta a_n(t) = +\infty$), Eq. (21) will not pass and thus neither mandatory nor discretionary LCs will not occur. When the current lane is not in the desired lane set and the target lane is in the desired lane set (i.e., $\Delta a_n(t) = -\infty$), Eq. (21) will always pass and thus mandatory LCs are considered by only checking Eqs. (19) and (20). Otherwise, the discretionary LCs are considered by checking both incentive and safety checks.

For simplicity, we assume that a LC completes immediately once it starts. Further, if a vehicle cannot change lane before L^{limit}, the vehicle will pass the intersection in the current lane and try to make LCs after passing the intersection.

(3) CAV car following model

Although the proposed TO will smooth trajectories, it does not guarantee that the planned trajectory is safe. For example, in Fig. 1, CAV n's planned trajectory will intersect with HV m's trajectory when HV m cuts in front of the CAV n. Therefore, there is a need for a safety feature to ensure the avoidance of collision. The safety feature is considered to follow a CAV car following model (e.g., Gipps' car following model with s_0^{CAV} and τ^{CAV}).

$$v_n\left(t+\tau^{\mathrm{CAV}}\right) = \begin{cases} F_{n,l_n(t)}^{\mathrm{CAV}}\left(v_n(t), v_{l_n(t)}(t), s_{n,l_n(t)}(t)\right), \\ \qquad\qquad \text{if } \operatorname{mod}(t, C) \in [0, G], \\ \min\left\{F_{n,l_n(t)}^{\mathrm{CAV}}\left(v_n(t), v_{l_n(t)}(t), s_{n,l_n(t)}(t)\right), F_{n,l_n(t)}^{\mathrm{CAV}}\left(v_n(t), 0, L + s_0^{\mathrm{CAV}} - x_n(t)\right)\right\}, \\ \qquad\qquad \text{otherwise.} \end{cases} \tag{23}$$

$$F_{n,l_n(t)}^{\mathrm{CAV}}\left(v_n(t), v_{l_n(t)}(t), s_{n,l_n(t)}(t)\right) = \min\left\{v_n(t) + \overline{a}\tau^{\mathrm{CAV}}, \overline{v}, v_{CAV}^{\mathrm{safe}}\left(v_{l_n(t)}(t), s_{n,l_n(t)}(t)\right)\right\}, \tag{24}$$

where $v_{CAV}^{\mathrm{safe}}\left(v_{l_n(t)}(t), s_{n,l_n(t)}(t)\right) = \underline{a}\tau^{\mathrm{CAV}} + \sqrt{\left(\underline{a}\tau^{\mathrm{CAV}}\right)^2 + v_{l_n(t)}(t)^2 + 2\underline{a} \times \left(s_{n,l_n(t)}(t) - s_0^{\mathrm{CAV}}\right)}$ is the safety speed of a CAV. Also, the CAV car following model can be applied in a no control scenario without any trajectory optimization.

As soon as the planned trajectory becomes safe again, the CAV will switch back to follow the planned trajectory. See Fig. 1, CAV n will first follow a planned trajectory generated from TO. However, due to the cut-in LC of HV $m \in \mathcal{N}^{\mathrm{HV}}$, CAV n will abandon the planned trajectory and then control its trajectory with the CAV car following model to ensure safety. Although it ensures that two consecutive vehicles do not collide, the planned trajectory of CAV n is affected by HV m's LCs and thus may weaken the expected system performance of TO with extra "stop-and-go" traffic.

3. Lane-change-aware trajectory optimization model

To address the above problem existing in TO, this section proposes a decentralized trajectory optimization model with a lane-change-aware mechanism (LCTO) to replace TO in the above trajectory planning module. The lane-change-aware mechanism will restrain discretionary LCs and yield to mandatory LCs.

The continuous LCTO is formulated based on the continuous TO considering additional constraints. For each CAV $n \in \mathcal{N}^{\mathrm{CAV}}$,

$$\text{CLCTO}: \min_{X_n} J_n(X_n) := \omega_m\left(t_n^+ - t_n^-\right) + \omega_a \int_{t_n^-}^{\overline{t_n^+}} a_n(t)^2 dt, \tag{25}$$

subject to the same constraints in the continuous TO (i.e., Eqs. (7)–(16)) and additional LC-aware constraints including a restraining strategy for discretionary LCs and a yielding strategy for mandatory LCs.

In LCTO, we estimate the type of LCs according to the following formulation.

When $x_n(t) \in [0, L^{\mathrm{limit}})$, we have

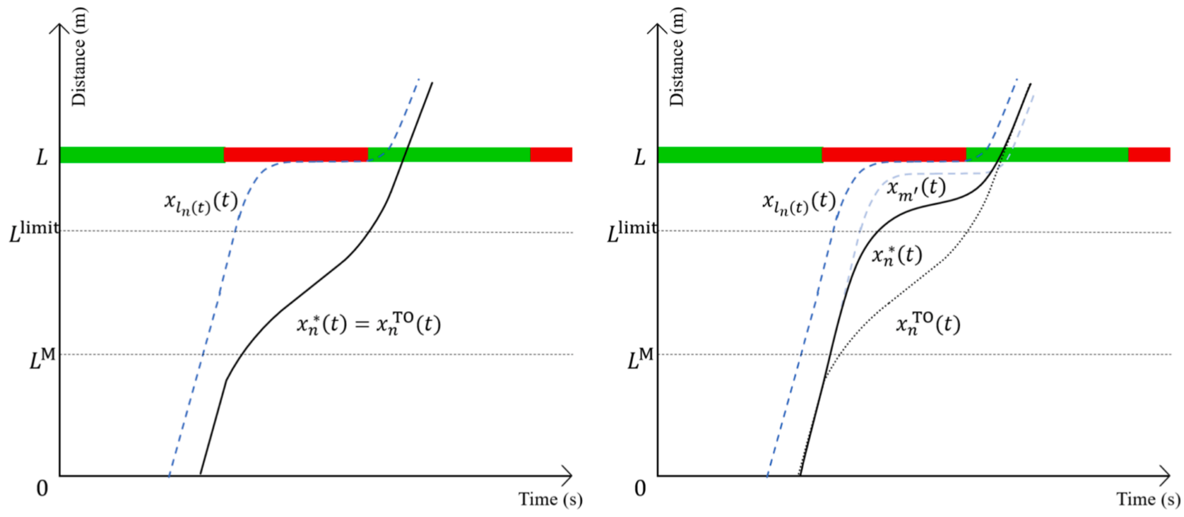

(a) Without cut-in LCs. (b) With cut-in LCs.

Fig. 4. Illustrations of Remark 1.

$$\Delta a_{m(t)}(t) = \begin{cases} +\infty, & \text{if } o_{m(t)}(t) \in \widehat{O}_{m(t)} \text{ and } o^*_{m(t)}\left(t\right) \notin \widehat{O}_{m(t)} \\ & \text{and } x_{m(t)}(t) \geqslant L^{\mathrm{M}}, \\ -\infty, & \text{if } o_{m(t)}(t) \notin \widehat{O}_{m(t)} \text{ and } o^*_{m(t)}\left(t\right) \in \widehat{O}_{m(t)} \\ & \text{and } x_{m(t)}(t) \geqslant L^{\mathrm{M}}, \\ 0.1, & \text{otherwise.} \end{cases} \tag{26}$$

$$\widehat{O}_{m(t)} = \left\{ \widetilde{O}_{m(t)}, \text{if } m\left(t\right) \in \mathcal{N}^{\mathrm{CHV}} \cup \mathcal{N}^{\mathrm{CAV}}, \{-1\}, \text{otherwise.} \right. \tag{27}$$

In Eq. (27), $\mathcal{N}^{\mathrm{CHV}}$ is the set of connected HVs and $\widehat{O}_{m(t)}$ is the estimated desired lane set of vehicle $m(t)$. If vehicle $m(t)$ is a connected vehicle, the estimated desired lane set is its desired lane set. Otherwise, it will be set as -1. Thus, we can predict the type of LCs based on Eq. (26). When $\Delta a_{m(t)}(t) = 0.1$, the discretionary LC occurs, otherwise the mandatory LC occurs. For those unconnected vehicles, their LCs are assumed to be the discretionary LCs and $\Delta a_{m(t)}(t) = 0.1$. For those connected vehicles, $\Delta a_{m(t)}(t)$ is calculated according to their types of LCs. Then, we introduce the LC-aware constraints with two types of LCs.

- LC-aware constraints: For discretionary LCs, a LC restraining strategy is executed by adding upper bounds of the following distance, which is formulated as follows,

$$(1-\beta_{m(t)}(t)) \times \left(x_{m(t)}\left(t\right) - x_n\left(t\right) - \left(s_0^{\mathrm{CAV}} + l^{\mathrm{veh}}\right) - \tau^{\mathrm{CAV}} v_n\left(t\right)\right) \leq 0,\ \forall t \in \left[t_n^-, \overline{t_n^+}\right], \tag{28}$$

where $\beta_{m(t)}(t)$ is an indicator whether HV $m(t) = \widehat{l}_n(t) \in \mathcal{N}^{\mathrm{HV}}$ (i.e., the preceding vehicle in the target lane) has a potential to make discretionary LCs at time $t \in \left[t_n^-, \overline{t_n^+}\right]$ and is formulated as follows.

$$\beta_{m(t)}\left(t\right) = \left\{ 0,\ \text{if } \widetilde{a}_{m(t),\widehat{l}_{m(t)}(t)}\left(t\right) - \widetilde{a}_{m,l_{m(t)}(t)}\left(t\right) > 0.1 \quad \text{or } s_{m(t),\widehat{l}_{m(t)}(t)}\left(t\right) > s_0^{\mathrm{HV}} + \tau^{\mathrm{HV}} v_{m(t)}\left(t\right), 1, \text{otherwise.} \right. \tag{29}$$

If $\beta_{m(t)}(t) = 1$, HV $m(t)$ does not have a potential to make discretionary LCs and Eq. (28) will always be 0. If $\beta_{m(t)}(t) = 1$, it indicates that either Safety Check 1 (Eq. (19)) or Incentive Check (Eq. (21)) does not pass, i.e., the discretionary LC will not happen. If $\beta_{m(t)}(t) = 0$, HV $m(t)$ has a potential to make discretionary LCs and Eq. (28) will only be determined by the Safety Check 2 (i.e., Eq. (20)). To restrain the discretionary LCs, the spacing between the CAV and its preceding vehicle in the target lane should be less than the safety spacing.

For mandatory LCs, a LC yielding strategy is provided to slow down the CAV n and let HV $m(t)$ make mandatory LCs. Since LCs are induced by the smoothed CAV trajectory (i.e., CAVs are slowed down) via TO, the yielding strategy will ask the CAV n to follow the

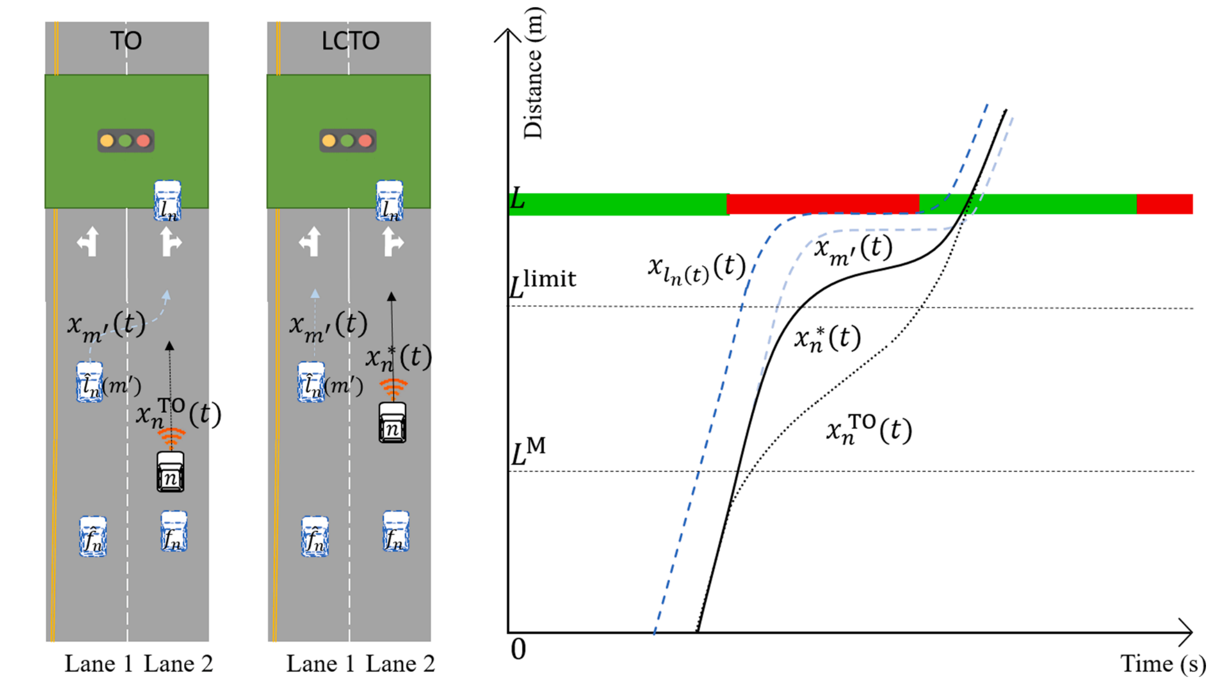

Fig. 5. An illustration of the LC-aware mechanism.

planned trajectory in TO. Thus, if it is a mandatory LC, $\beta_{m(t)}(t) = 1$ as well.

Because $m(t)$ is time-variant, Eqs. (28) - (26) are nonlinear. To linearize LC-aware constraints, $\mathcal{P}_n(t) := \{m' | x_n(t) \leqslant x_{m'}(t) \leqslant x_{l_n(t)}(t), \forall o_{m'}(t) \neq o_n(t)\}, \forall n \in \mathcal{N}^{\mathrm{CAV}}$, is defined as a preceding vehicle set that includes vehicles in adjacent lanes located between the preceding vehicle $l_n(t)$ and CAV n at time t.

Remark 1. If the optimal trajectory $x_n^{\mathrm{TO}}(t)$ of CAV n at time $t \in [t_n^-, t_n^+]$ in TO and the optimal solution $x_n^*(t)$ in LCTO exist, then $x_n^*(t) \geqslant x_n^{\mathrm{TO}}(t)$.

Proof. Without LC restraining constraints, see Fig. 4, TO has the optimal solution $x_n^{\mathrm{TO}}(t), \forall t \in [t_n^-, t_n^+]$ (i.e., the black-dotted curve). With LC restraining constraints, if there is no potential for HVs on the adjacent lane to make LCs in front of CAV n, then $x_n^*(t) = x_n^{\mathrm{TO}}(t)$ (i.e., black-solid curve); otherwise, the trajectory of CAV n should be closer to HV m' (i.e., the gray-dashed curve in Fig. 4 (b)) to restrain LCs, i.e., $x_n^*(t) > x_n^{\mathrm{TO}}(t)$. Thus, $x_n^*(t) \geqslant x_n^{\mathrm{TO}}(t)$. This completes the proof. □

Then, $\mathcal{P}_n(t) := \{m' | x_n^{\mathrm{TO}}(t) \leqslant x_{m'}(t) \leqslant x_{l_n(t_n^-)}(t), \forall o_{m'}(t) \neq o_n(t)\}$. To restrain discretionary LCs, we can find the first vehicle that has potential to make discretionary LCs in $\mathcal{P}_n(t)$, i.e., $p_n(t) = \mathrm{argmax}_{k \in \mathcal{P}_n(t)}(x_k(t) | \beta_k(t) = 0)$.

Remark 2. If LCs of vehicle $p_n(t)$ are restrained, then the other vehicles in $\mathcal{P}_n(t)$ cannot change lanes in front of CAV n.

Proof. Let $p_n'(t)$ be the nearest following vehicle of vehicle $p_n(t)$, then $x_{p_n(t)}(t) - x_{p_n'(t)}(t) > l^{\mathrm{veh}} + s_0^{\mathrm{HV}} + \tau^{\mathrm{HV}} v_{p_n'(t)}(t)$. If vehicle $p_n(t)$ cannot make LCs in front of CAV n, we have $x_{p_n(t)}(t) - x_n(t) \leqslant l^{\mathrm{veh}} + s_0^{\mathrm{CAV}} + \tau^{\mathrm{CAV}} v_n(t)$. Combined these two equations, we have $x_{p_n'(t)}(t) < x_{p_n(t)}(t) - \left(l^{\mathrm{veh}} + s_0^{\mathrm{HV}} + \tau^{\mathrm{HV}} v_{p_n'(t)}(t)\right) \leqslant x_n(t) + l^{\mathrm{veh}} + s_0^{\mathrm{CAV}} + \tau^{\mathrm{CAV}} v_n(t) - \left(l^{\mathrm{veh}} + s_0^{\mathrm{HV}} + \tau^{\mathrm{HV}} v_{p_n'(t)}(t)\right)$, i.e., $x_{p_n'(t)}(t) - x_n(t) < l^{\mathrm{veh}} + s_0^{\mathrm{CAV}} + \tau^{\mathrm{CAV}} v_n(t)$. Thus, this completes the proof. □

With Remarks 1 and 2, we only need to consider vehicle $p_n(t)$ at time t in Eqs. (28) and (29), and to reformulated them as follows,

$$\left(1 - \beta_{p_n(t)}(t)\right) \times \left(x_{p_n(t)}(t) - x_n(t) - \left(s_0^{\mathrm{CAV}} + l^{\mathrm{veh}}\right) - \tau^{\mathrm{CAV}} v_n(t)\right) \leq 0, \ \forall t \in [t_n^-, t_n^+]. \tag{30}$$

$$\beta_{p_n(t)}\left(t\right) = \begin{cases} 0, & \text{if } \tilde{a}_{p_n(t), \hat{l}_{p_n(t)}(t)}\left(t\right) - \tilde{a}_{p_n(t), l_{p_n(t)}(t)}\left(t\right) > 0.1 \quad \text{or } s_{p_n(t), \hat{l}_{p_n(t)}(t)}\left(t\right) > s_0^{\mathrm{HV}} + \tau^{\mathrm{HV}} v_{p_n(t)}\left(t\right), \\ 1, & \text{otherwise.} \end{cases} \tag{31}$$

Because $p_n(t)$ is known at any time t, $\beta_{p_n(t)}(t)$ and $x_{p_n(t)}(t)$ are known and thus Eq. (30) is linear. Fig. 5 plots an illustration of the LC-aware mechanism. In TO, the HV m' will change lanes in front of the CAV n. If the discretionary LC occurs, the discretionary LC

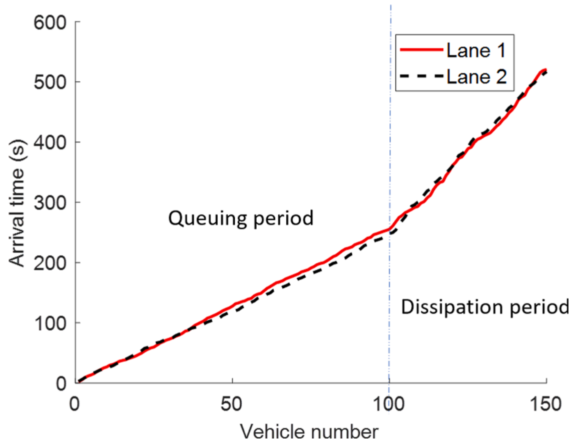

Fig. 6. An example of the arrival patterns.

restraining strategy will shorten the spacing between the CAV n and its preceding vehicle in the same lane l_n. If the mandatory LC occurs, the mandatory LC yielding strategy will ask the CAV n to follow the planned trajectory in TO (i.e., slow down to yield larger space for mandatory LCs).

According to Fig. 2, the motions of downstream vehicles are rarely affected by upstream traffic, and thus, the sub-problems will be solved sequentially from the lead CAV to the last CAV. In each sub-problem, LCTO will be activated when CAV m arrives the control zone. The locations, speeds and occupied lanes of preceding vehicles are known (CAVs follow the planned trajectories generated in LCTO, and HVs follow the HV car following model in Eqs. (17) and (18) and the lane changing model in Eqs. (19)–(21). Then, we can estimate the departure time of vehicle m, and construct LC-aware constraints with the solution from TO and obtain CAV m's trajectory by solving LCTO. Note that LCTO only works within the approaching road segment. Once a CAV passes the intersection, it follows the CAV car following model (i.e., Eqs. (23) and (24)).

Since the continuous TO and LCTO models are difficult to be solved as the continuous time points where decision variables dwell lead to infinite dimensionality, the continuous TO and LCTO will be formulated as discrete models to find the exact optimal solutions in numerical experiments. The discrete TO and LCTO are shown in Appendix B.

4. Numerical experiments

This section conducts a set of numerical experiments to test the performance of TO and LCTO. The numerical experiments are conducted using Matlab on a PC with 3.6 GHz Intel Core i7 CPU, 16 GB RAM. The parameter settings are described in SubSection 4.1. SubSection 4.2 analyzes the effects of CAV market penetration on TO, LCTOY, and LCTO at a signalized intersection with multi-lane roads. SubSection 4.3 investigates the system sensitivity performance of LCTO with varying road segment lengths, signal cycle lengths, traffic saturation rates and through-vehicle rates at a signalized intersection with multi-lane roads.

4.1. Parameter settings

Parameters are set to the following default values. The simulation time is $T = 800$ s and the time interval is $\Delta t = 0.1$ s. The road segment length is $L = 500$ m and the number of lanes is $K = 2$. We consider the first 150 vehicles in each lane that are evenly distributed, and thus the total number of vehicles is $N = N \times K = 300$ veh. The vehicle length is $l^{\text{veh}} = 4$ m. The speed limit is $\bar{v} = 16$ m/s. The maximum acceleration is $\bar{a} = 2$ m/s^2 and the minimum acceleration is $\underline{a} = -2$ m/s^2. LCs are forbidden after location $L^{\text{limit}} = L + \bar{v}^2/2\underline{a}$, and mandatory LCs occur after location $L^{\text{M}} = L^{\text{limit}/2}$. The minimum spacing and time gap of a CAV are $s_0^{\text{CAV}} = 1$ m and $\tau^{\text{CAV}} = 0.7$ s respectively. The minimum spacing and time gap of an HV are $s_0^{\text{HV}} = 4$ m and $\tau^{\text{HV}} = 1$ s respectively. The signal cycle length is $C = 60$ s and the effective green length is $G = C/2$. The through-vehicle rate, left-vehicle rate and right-vehicle rate are $\epsilon^{\text{T}} = 0.6$, $\epsilon^{\text{L}} = 0.2$ and $\epsilon^{\text{R}} = 0.2$, respectively. The CAV MPR in lane 1 is $MPR_1 = 50\%$ and the CAV MPR in lane 2 is $MPR_2 = 50\%$. The weight of squared acceleration $\omega_a = 1$ and weight of mobility $\omega_m = 1$. The detail of weight selection is shown in Appendix C. To better reflect the reality, we divide the traffic into two parts according to Sun et al. (2015): the queuing period (e.g., the first 2/3 vehicles in each lane) when "stop-and-go" traffic occurs seriously at high traffic saturation rates; and the dissipation period (e.g., the last 1/3 vehicles in each lane) when the "stop-and-go" traffic is dissipating gradually at low traffic saturation rates (set as 0.5 in this study). In the queuing period, the traffic saturation rate in lane 1 is $f_1^s = 1$ and the traffic saturation rate in lane 2 is $f_2^s = 1$. Further, the arrival times and arrival speeds are generated from Eqs. (3)–(5). Fig. 6 depicts an example of the arrival patterns with the queuing and dissipation periods. The traffic flows are about 1440 veh/h and 720 veh/h in the queuing period with $f^s = 1$ and the dissipation period with $f^s = 0.5$, respectively. Due to a higher traffic saturation rate in the queuing period, the slope in the queuing period is smaller than that in the dissipation period; i.e., vehicles arrive with smaller time gaps in the queuing period than those in the dissipation period.

Table 1
Coefficients for fuel consumption. Note that the units of fuel consumption, speed and acceleration are in l, m/s, and m/s^2, respectively.

$\kappa_{j_1 j_2}$	$j_2 = 0$	$j_2 = 1$	$j_2 = 2$	$j_2 = 3$
$j_1 = 0$	−7.537	0.4438	0.1716	−0.0420
$j_1 = 1$	0.0973	0.0518	0.0029	−0.0071
$j_1 = 2$	−0.0030	−7.42E−4	1.09E−4	1.16E−4
$j_1 = 3$	5.3E−5	6E−6	−1E−5	−6E−6

In the numerical experiments, the following indicators are adopted to measure the system performance.

- Riding comfort: The summation of squared acceleration is used to measure the system riding comfort.

$$\overline{SA} = \frac{\sum_{n=1}^{N} \sum_{i=i_n^-}^{i_n^+} (a_n[i])^2 \Delta t}{N}, \tag{32}$$

where $\overline{SA}$ is the average system squared acceleration. Lower value of the system squared acceleration means less sharp acceleration, and thus yields more riding comfort.

- Travel time: The summation of all vehicles' travel time during road segment L is used to measure the system travel time.

$$\overline{TT} = \frac{\sum_{n=1}^{N} \left(t_n^+ - t_n^-\right)}{N}, \tag{33}$$

where $\overline{TT}$ is the average system travel time. Lower value of the system travel time means better traffic mobility.

- Fuel consumption: The summation of the instantaneous fuel consumption function (i.e., the VT-micro model used in Ma et al. (2017)) is used to measure the system fuel consumption.

$$\overline{FC} = \frac{\sum_{n=1}^{N} \sum_{i=i_n^-}^{i_n^+} \exp\left\{ \sum_{j_1=0}^{3} \sum_{j_2=0}^{3} \kappa_{j_1 j_2} (v_n[i])^{j_1} (a_n[i])^{j_2} \right\} \Delta t}{N}, \tag{34}$$

where $\overline{FC}$ is the average system fuel consumption. j_1 and j_2 are the power indexes. $\kappa_{j_1 j_2}$ is a constant coefficient. See Table 1 for the value of the coefficients (Zegeye et al., 2013). Lower value of the system fuel consumption means better fuel efficiency.

- Safety: The system safety is measured by a safety surrogate (i.e., the inverse time-to-collision) described in Gettman and Head (1840) and Ma et al. (2017).

$$\overline{SS} = \frac{\sum_{n=1}^{N} \sum_{i=i_n^-}^{i_n^+} \max\left\{ 0, \frac{v_n[i] - v_{l_n[i]}[i]}{x_{l_n[i]}[i] - x_n[i] - l^{\text{veh}}} \right\} \Delta t}{N}, \tag{35}$$

where $\overline{SS}$ is the average system safety surrogate. Eq. (35) is compatible with leading vehicles because of $v_{l_{n'}[i]} = \overline{v}$ and $x_{l_{n'}[i]} = \infty$, $\forall n' \in \mathcal{N}'$. Lower value of the system safety surrogate means less potential of collision, and thus yields safer riding experience.

Further, five scenarios are conducted in the numerical experiments for comparison.

1) CF (benchmark): HVs follow Gipps' car following and lane changing models; CAVs follow the CAV car following model. In this scenario, the trajectory optimization model is not activated, and vehicles will follow their own driving behaviors (e.g., car following and lane changing).

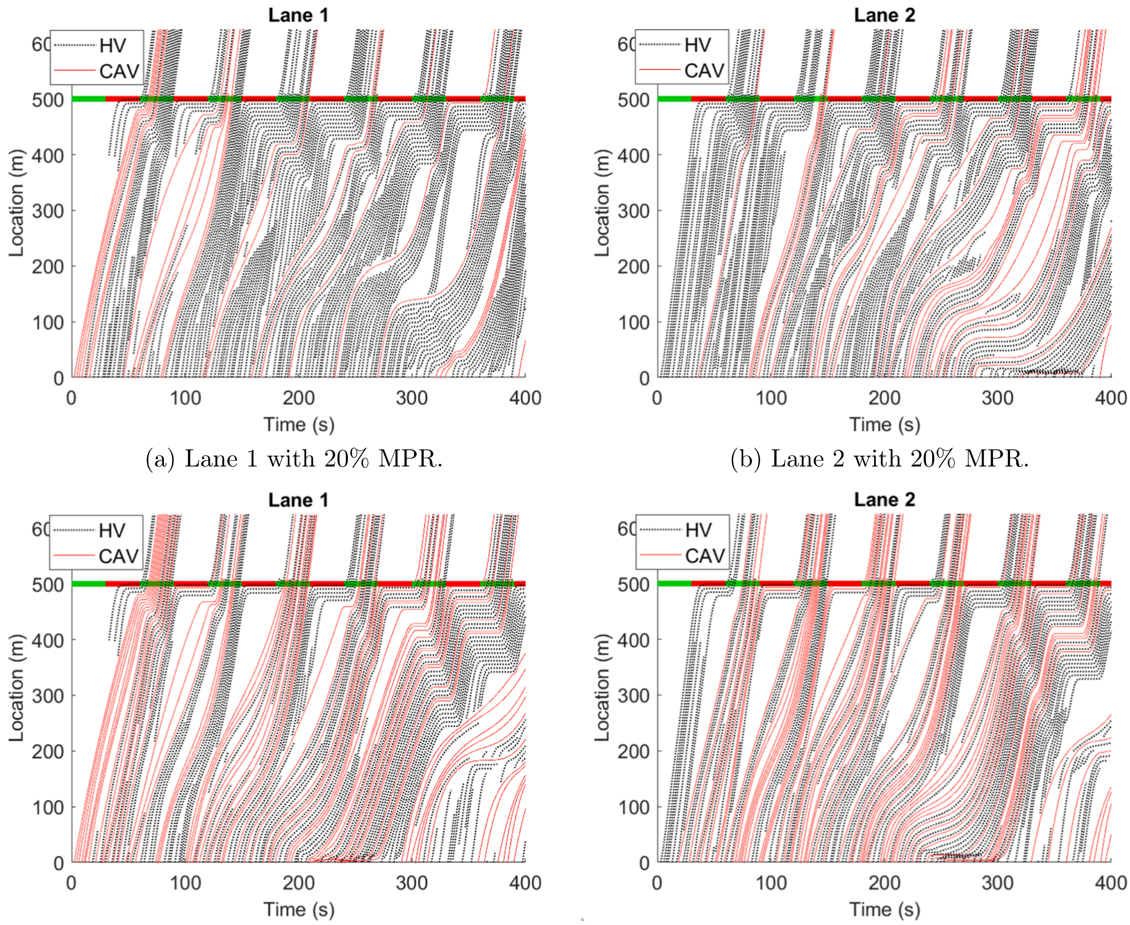

(a) Lane 1 with 20% MPR. (b) Lane 2 with 20% MPR.

(c) Lane 1 with 50% MPR. (d) Lane 2 with 50% MPR.

Fig. 7. Examples of trajectory results in TO.

2) TO: HVs follow Gipps' car following and lane changing models; CAVs follow the planned trajectories generated in TO model and the CAV car following model. In this scenario, the trajectory optimization model is focusing on longitudinal maneuver without considering the lane-change-aware mechanism.
3) LCTO: HVs follow Gipps' car following and lane changing models; CAVs follow the planned trajectories generated in LCTO model and the CAV car following model. In this scenario, the lane-change-aware mechanism is activated in the trajectory optimization model.
4) TOWOLC: HVs follow Gipps' car following model without considering the lane changing behavior; CAVs follow the planned trajectories generated in TO model. In this scenario, the trajectory optimization model is not affected by the lateral maneuver (e.g., lane changing).
5) TOLCY: HVs follow Gipps' car following and lane changing models; CAVs follow the planned trajectories generated by a trajectory optimization with the LC yielding strategy (i.e., the cooperative LC strategy) based on the previous studies (Ko and Chang, 2018; Zhang et al., 2018; Chen et al., 2020). In this scenario, the trajectory optimization model requires CAVs yielding spacing to HV cut-in LCs.

4.2. CAV market penetration analysis

This subsection investigates CAV market penetration impacts on TO, LCTOY, and LCTO at a signalized intersection with two-lane roads. We assume that $MPR = MPR_1 = MPR_2$ and MPR is set to vary from 10% to 100% with an increment of 10%. The other parameters are fixed at their default values, respectively. Note that we also investigate the performance of LCTO at a signalized intersection with three-or-more-lane roads, which shows a similar result as in the two-lane experiments. The detail is shown in Appendix D.

Figs. 7–9 plot examples of trajectories in TO, LCTOY, and LCTO, respectively. When the CAV MPR is low (e.g., 20%), as shown in Fig. 7 (a) and (b), a number of HVs change lanes in front of CAVs due to the large gaps induced by TO. When the CAV MPR grows to 50%, as shown in Fig. 7 (c) and (d), only a few HVs change lanes in front of CAVs. We also find these LCs might cause extra "stop-and-

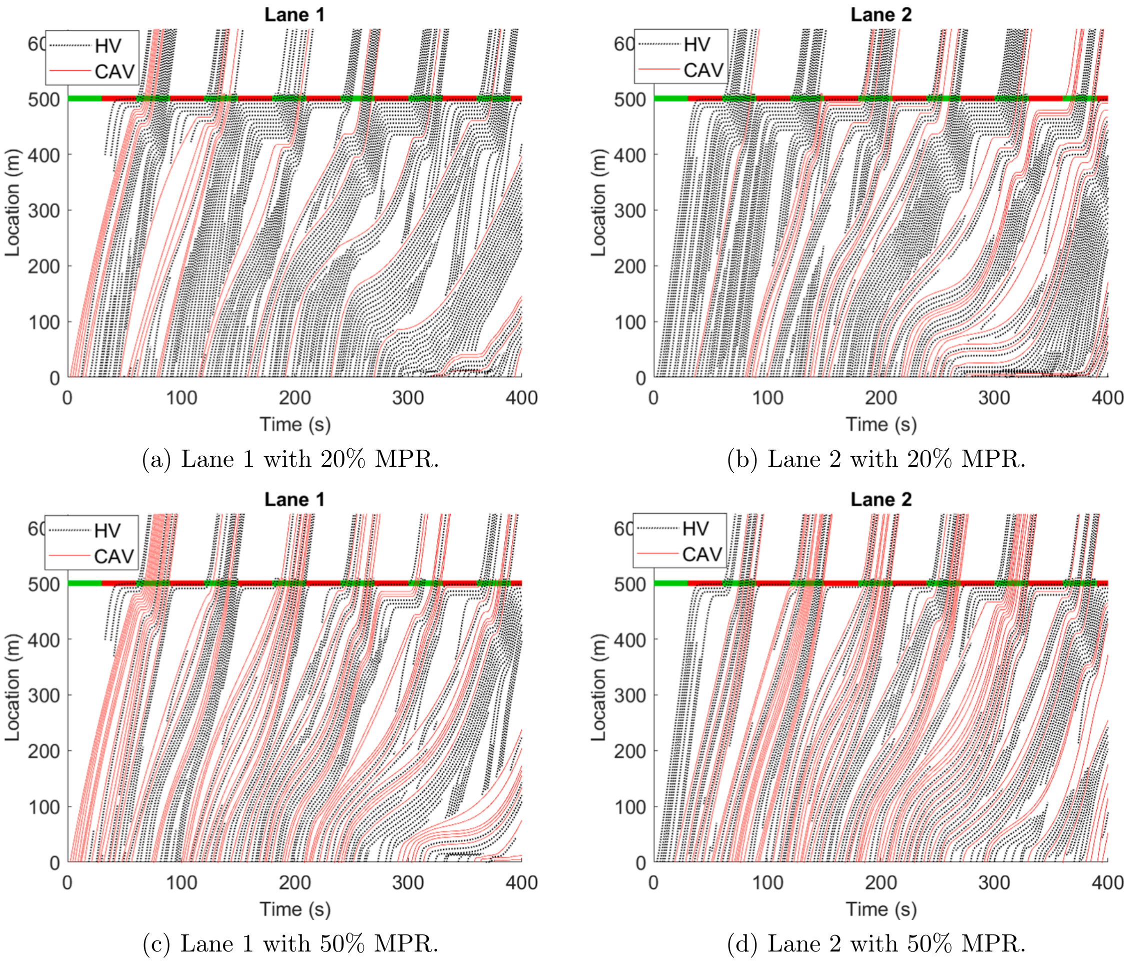

(a) Lane 1 with 20% MPR. (b) Lane 2 with 20% MPR.

(c) Lane 1 with 50% MPR. (d) Lane 2 with 50% MPR.

Fig. 8. Examples of trajectory results in LCTOY.

go" traffic and "spillback" traffic in TO. Additionally, as shown in Fig. 8, LCTOY yields more "stop-and-go" traffic and "spillback" at a lower CAV MPR and smoother trajectories at a higher CAV MPR. However, in Fig. 9, we find less LCs, less "stop-and-go" traffic and no "spillback" traffic in LCTO compared with those in TO and LCTOY.

Then, we plot the benefits of the system performance with varying CAV MPRs in Fig. 10. The system joint objective, LC frequency per vehicle, the system riding comfort, the system travel time, the system fuel consumption and the system safety are considered. The gray-dotted curve denotes the benefits of the system performance in TOWOLC compared with those in CF. The black-solid curve denotes the benefits of the system performance in TO compared with those in CF. The red-dashed curve denotes the benefits of the system performance in LCTO compared with those in CF. The green-dash-dotted curve denotes the benefits of the system performance in LCTOY compared with those in CF. The yellow bars denote the extra benefits of the system performance in LCTO compared with those in TO.

See Fig. 10 (a), we find that the benefits of the system joint objective in both TO, LCTOY, and LCTO increase with the increasing CAV MPRs. The benefits are about 15% at a low CAV MPR (e.g., 10%), and reach to 70% after the CAV MPR exceeds 80%. The benefits are relatively low due to the predominance of HVs in mixed traffic when the CAV MPR is low. From Fig. 10 (b), we find that the LC frequencies per vehicle in TO, LCTOY and LCTO are higher at a low CAV MPR than those at a high CAV MPR. This is consistent with Yang et al. (2017), because there are less gaps for HVs to change lanes when more CAVs follow the planned trajectories at a higher CAV MPR. Additionally, note that TOWOLC provides the upper bound of the expected benefits of trajectory smoothing without considering LCs. The expected benefits in TOWOLC could be significant when the CAV MPR is relatively low (e.g., 50% in the system joint objective, riding comfort, and safety, 30% in the system fuel consumption, as well as 10% in the system travel time when the CAV MPR is only 10%). However, the presence of LCs will significantly impair the expected benefits. Comparing TOWOLC with TO, we see that the expected benefits are decreased half or more due to actual HV LCs. Therefore, it is necessary to restrain or yield the HV LCs for improving the system performance.

We see that the performance of LCTOY is worse than TO at a lower CAV MPR (e.g., lower than 30%), and becomes better at a higher CAV MPR. This is probably because that LCTOY will yield more space to HV LCs. When the CAV MPR is low, "stop-and-go" traffic and

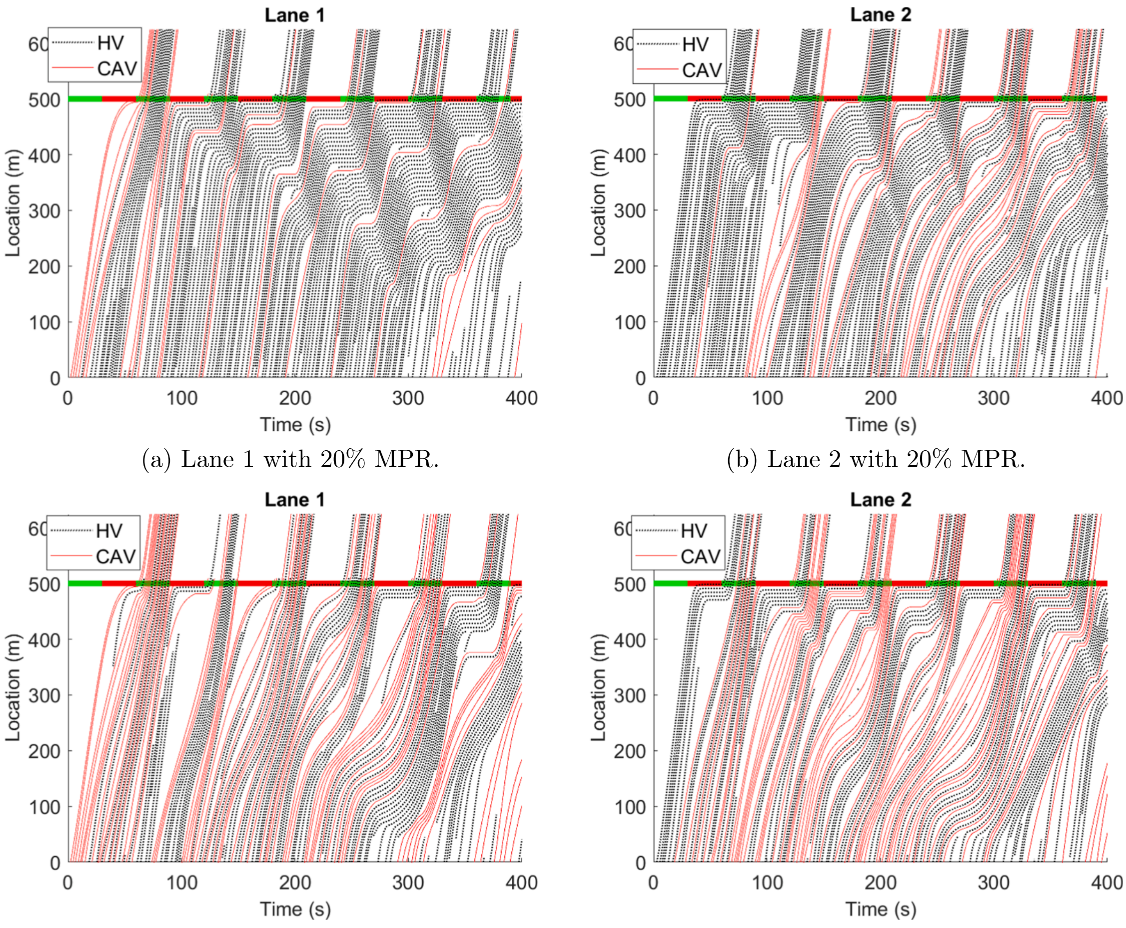

(a) Lane 1 with 20% MPR. (b) Lane 2 with 20% MPR.

(c) Lane 1 with 50% MPR. (d) Lane 2 with 50% MPR.

Fig. 9. Examples of trajectory results in LCTO.

"spillback" traffic become heavier due to more space yielded in LCTOY, as shown in Fig. 8 (a) and (b). When the CAV MPR is high, more CAVs are controlled and less "stop-and-go" traffic and "spillback" traffic happen, as shown in Fig. 9 (c) and (d).

Compared LCTO with TO, as shown in Fig. 10 (a), the extra benefit of the system objective in LCTO increases first at low CAV MPRs and then decreases at high CAV MPRs. The LC frequencies per vehicle in Fig. 10 (b) explain this observation: 1) Although more LCs occur at a low CAV MPR, the effects of both TO and LCTO are weak due to the predominance of HVs and thus LCTO yields less extra benefits; 2) When the CAV MPR grows, there still exist more LCs occurred in TO than in LCTO, and both TO and LCTO yield significant benefits, and thus LCTO yields more extra benefits by restraining these LCs; 3) When the CAV MPR further grows, more CAVs follow the planned trajectories with less gaps, and less or no LCs are induced by TO, and thus LCTO yields less extra benefits. Therefore, we say that LCTO shows much better performance than TO and LCTOY due to the restraining strategy for discretionary LCs and the yielding strategy for mandatory LCs.

Additionally, Fig. 10 (c) - (f) show that the benefits of the system riding comfort, travel time, fuel consumption and safety in TO and LCTO increase as the CAV MPR increases, and the extra benefits of the system riding comfort, travel time, fuel consumption and safety in LCTO show similar trends as the system joint objective. Because the system joint objective integrates the system riding comfort and mobility (i.e., travel time surrogate), thus the benefits of the system riding comfort and travel time increase accordingly. However, the benefit of the system travel time is negative when the CAV MPR is lower than 50%. This is because that HVs change lanes with a purpose of acquiring mobility advantages, and thus the system travel time in CF might be smaller than that in TO/LCTO when the CAV MPR is low (Li et al., 2021). Also, the benefits of the system travel time in both TO and LCTO are a little higher at 10% CAV MPR than those at 20% CAV MPR. This is probably because the benefits of both TO and LCTO are relatively insignificant at a extremely low CAV MPR and HVs change lanes at a purpose of obtaining mobility advantage, and thus the system travel time is higher at a lower CAV MPR. When the CAV MPR is high, there are more CAVs in the system and they will follow the planned trajectories to improve the system travel time. Also, we find that the system fuel consumption and safety are related to accelerations in Eq. (34). Thus, the system fuel consumption and safety are also improved by optimizing the system joint objective. Note that the extra benefit of the system fuel consumption in LCTO is marginal. Because the system fuel consumption is not only related to accelerations but also to speeds, and thus

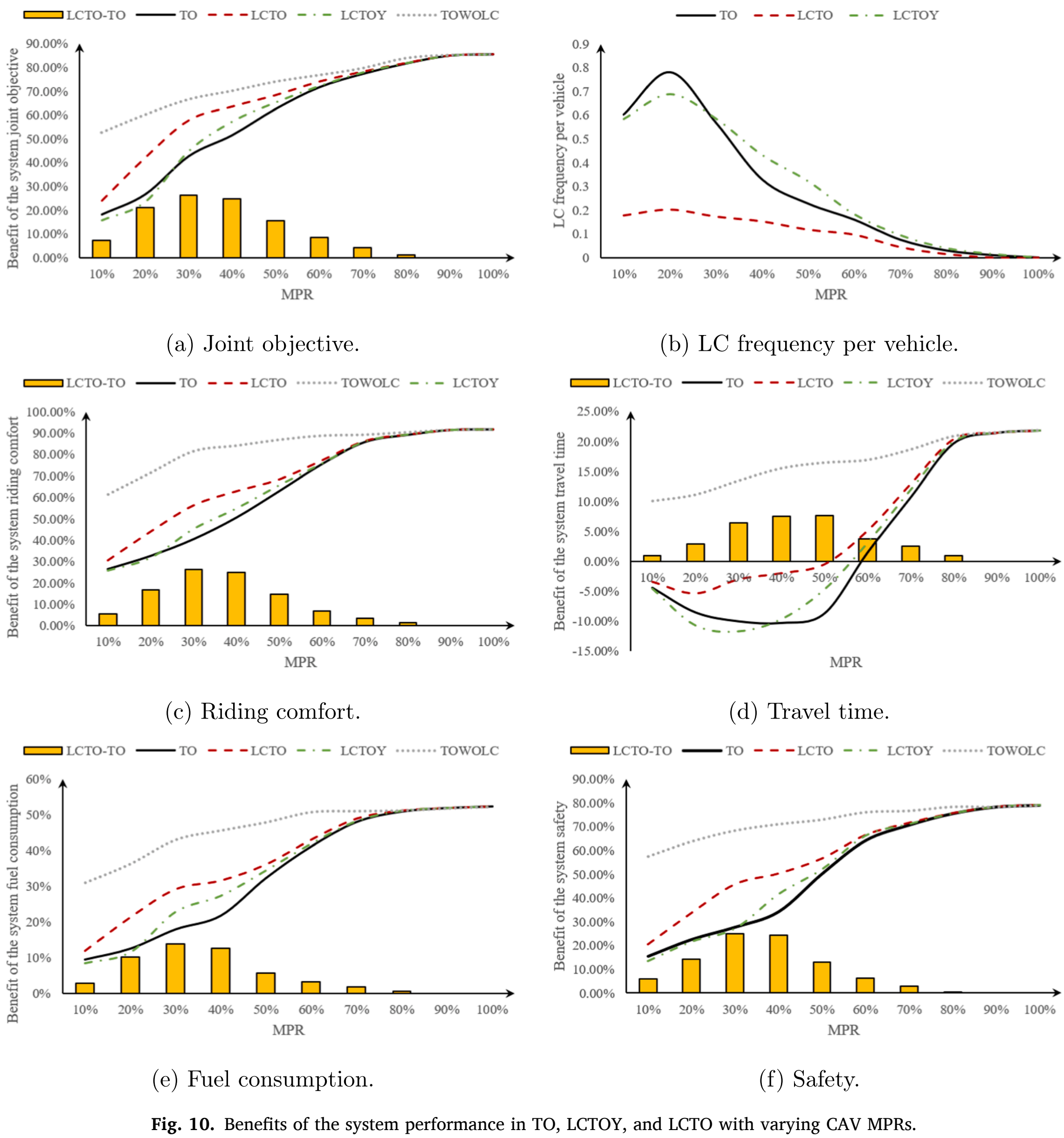

(a) Joint objective. (b) LC frequency per vehicle.

(c) Riding comfort. (d) Travel time.

(e) Fuel consumption. (f) Safety.

Fig. 10. Benefits of the system performance in TO, LCTOY, and LCTO with varying CAV MPRs.

we might need to use a fuel consumption model instead of the squared acceleration in the objective function for yielding more benefits in the system fuel consumption.

Further, the computation time for each CAV in TO is less than 1 s (average value of 0.67 s), and LCTO takes a computation time (average value of 1.56 s) more than twice of that of TO on average. This is because that TO is nested in LCTO with Eqs. (43)–(45). Overall, TO and LCTO are able to be implemented in real-time applications with an edge computing framework that distributes the computation to each individual on board computers. In implementation, it is expected that LCTO yields more benefits in the system joint objective, riding comfort, travel time, fuel consumption and safety when the CAV MPR is lower than 80%. TO is suggested to be used for a higher computational efficiency with a similar system performance in LCTO when the CAV MPR is higher than 80%.

4.3. Sensitivity analysis on other parameters

In this subsection, the system sensitivity analyses of TO and LCTO are investigated with varying parameters. Figs. 11–14 plot the benefits of the system joint objective in TO and LCTO with varying road segment lengths, signal cycle lengths, traffic saturation rates and through-vehicle rates, respectively. The black-solid curve denotes the benefit of TO compared with CF, the red-dashed curve denotes the benefit of LCTO compared with CF. The yellow bars show the extra benefits of LCTO compared with TO. The black and gray bars show the LC frequencies per vehicle in TO and LCTO, respectively.

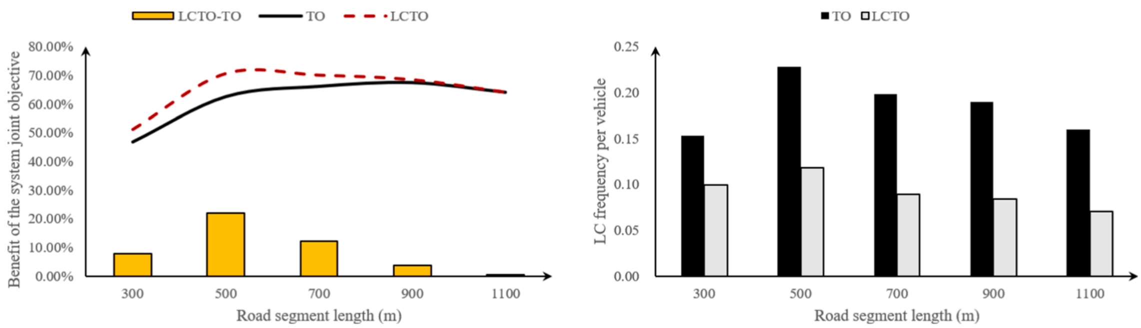

(a) Joint objective. (b) LC frequency per vehicle.

Fig. 11. Benefits of the system performance in TO and LCTO with varying road segment lengths.

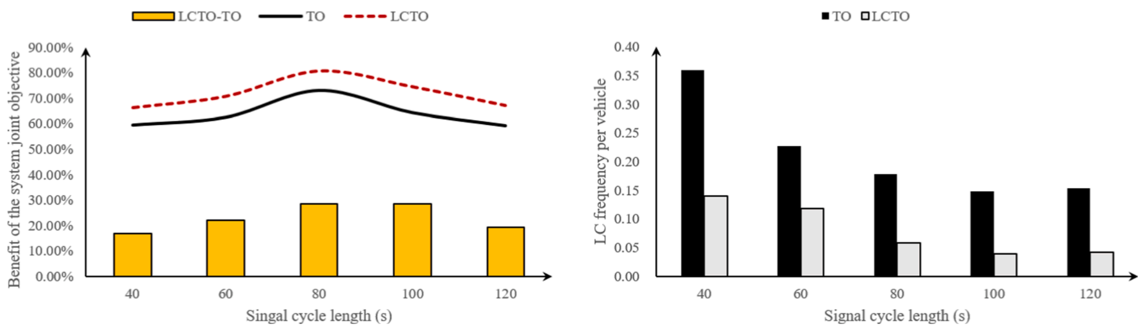

(a) Joint objective. (b) LC frequency per vehicle.

Fig. 12. Benefits of the system performance in TO and LCTO with varying road segment lengths.

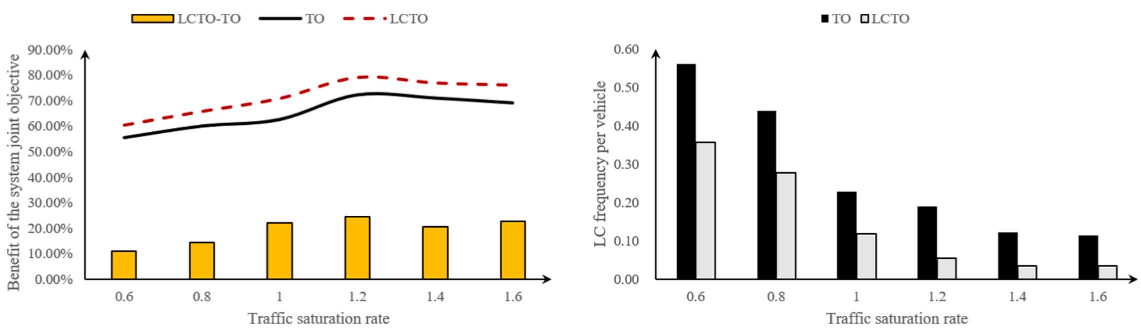

(a) Joint objective. (b) LC frequency per vehicle.

Fig. 13. Benefits of the system performance in TO and LCTO with varying traffic saturation rates.

1) Road segment length

We vary the road segment length range between 300 m and 1100 m with an increment of 200 m while fixing the other parameters at their default values. Compared with CF, as shown in Fig. 11 (a), the benefit of TO first grows with the increasing road segment length, and then drops a little as the road segment length further increases. From Fig. 11 (b), we find that the reason is probably that there is more "stop-and-go" traffic when the road segment is shorter, and the LC frequency increases with more room when the road segment length increases from a relatively short initial length. With a further increase of the road segment length, the "stop-and-go" traffic and the LC frequency per vehicle are less, and thus TO yields less benefits. Compared with TO, the extra benefit of LCTO first increases when the road segment length increases at low road segment lengths and then decreases with the further increasing road segment length. This is because that there exist less LCs in TO when the road segment length is extremely short, and LCTO yields less extra benefits. As the road segment length further increases, there are less "stop-and-go" traffic and less LCs. Thus, LCTO has a similar

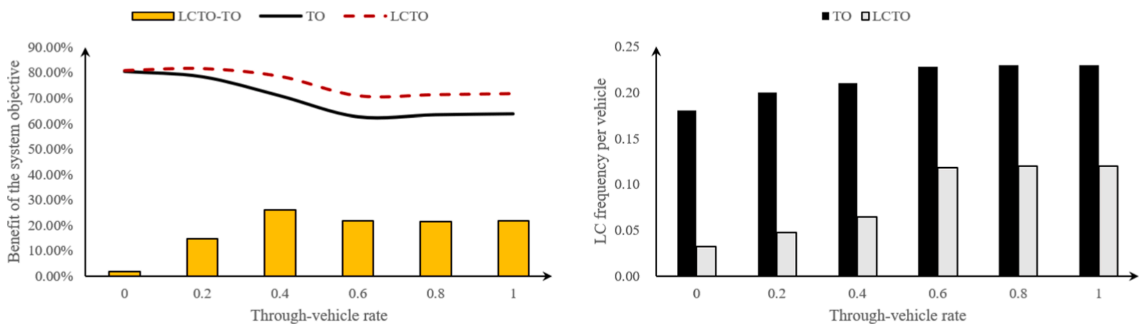

(a) Joint objective. (b) LC frequency per vehicle.

Fig. 14. Benefits of the system performance in TO and LCTO with varying through vehicle rates.

performance as TO when the road segment length is long. Overall, LCTO is better than TO when the road segment length is not relatively long (10–20% extra benefits).

2) Signal cycle length

We vary the signal cycle length between 40 s and 120 s with an increment of 20 s while fixing the other parameters at their default values. Compared with CF, as shown in Fig. 12 (a), the benefit of the system joint objective in TO grows first at low signal cycle lengths and then drops as the signal cycle length further increases. This is because a longer signal cycle length means that more vehicles can pass the intersection per signal cycle and yield less "stop-and-go" traffic. This is consistent with the findings in Xia et al. (2013), and thus TO has less potential to improve the system performance. Further, when the signal cycle length is short, the speed variation is smaller and thus the benefit in TO is less. Compared with TO, the extra benefit of LCTO increases at low signal cycle lengths, and then decreases with the further increasing signal cycle lengths. From Fig. 12 (b), we find that the LC frequencies per vehicle decrease as the signal cycle length increases. This is probably because "stop-and-go" traffic occurs more at a lower signal cycle length (i.e., vehicles may need to wait for several signal cycles in the queue before passing the intersection), and more HVs change lanes to avoid slower preceding vehicles. By restraining LCs induced by TO, LCTO increases the extra benefits at low signal cycle lengths. Then, with the further increasing signal cycle length, there are less "stop-and-go" traffic and less LCs induced by TO, and thus the extra benefit of LCTO decreases. Overall, the results suggest to use LCTO in different signal cycle lengths to yield extra benefits (15–30%).

3) Traffic saturation rate

We vary the traffic saturation rate in the queuing period between 0.6 and 1.6 with an increment of 0.2 and the traffic saturation rate in the dissipation period remains 0.5. The other parameters are fixed at their default values. Compared with CF, as shown in Fig. 13 (a), the benefit of TO first grows as the traffic saturation rate initially increases, and then drops a little at higher traffic saturation rates. Because there is less "stop-and-go" traffic and TO yields less benefits when the traffic saturation rate is lower. When the traffic saturation rate is higher, there is less room for TO to regulate LCs. Compared with TO, the extra benefit of LCTO increases at low traffic saturation rates, and then decreases a little at higher traffic saturation rates. From Fig. 13 (b), we find that the LC frequency per vehicle is higher due to more room in both TO and LCTO when the traffic saturation rate is lower. As the traffic saturation rate increases, LCTO yields more extra benefits by restraining the LCs induced by TO. In implementation, LCTO is expected to yield extra benefits (10–25%) across all traffic saturation rates.

4) Through-vehicle rate

We vary the through-vehicle rate range between 0 and 1 with an increment of 0.2 while fixing the other parameters at their default values. We also assume $\epsilon^{\mathrm{L}} = \epsilon^{\mathrm{R}} = \left(1 - \epsilon^{\mathrm{T}}\right)/2$. Compared with CF, as shown in Fig. 14 (a), the benefit of TO drops with the increasing through-vehicle rates. Because turn vehicles will not change lanes once they are in their desired lanes in the mandatory LC zone, but through vehicles will change lanes with the discretionary lane changing behavior before approaching L^{limit}. Thus, the LC frequency per vehicle grows as the through-vehicle rate increases, as shown in Fig. 14 (b). And the benefit of TO decreases due to more LCs. Compared with TO, the extra benefit of LCTO increases at low through-vehicle rates, and then decreases a little with the further increasing through-vehicle rate. Because LCTO restrains more LCs induced by TO to yield more benefits when the through-vehicle rate is low. When the through-vehicle rate increases to a high level, a number of LCs that are not induced by TO exist in both TO and LCTO, and thus the extra benefit of LCTO decreases a little. Only considering the through-vehicle rate, LCTO is suggested to be applied when the through-vehicle rate is not extremely low (10–25% extra benefits).

In summary, the above results suggest that using LCTO to restrain LCs induced by TO will yield extra benefits in most traffic scenarios except those when the road segment length is relatively long and the through-vehicle rate is relatively low.

5. Limitations and discussions

From the above numerical experiment results, LCTO is capable to restrain HV LCs induced by TO at a signalized intersection with multi-lane roads. However, the applicability of LCTO is limited to certain scenarios (e.g., a limited lane-change-aware mechanism, isolated intersections, fixed (or predictable) signal timing, and cyber-physical constraints). This section summarizes these limitations

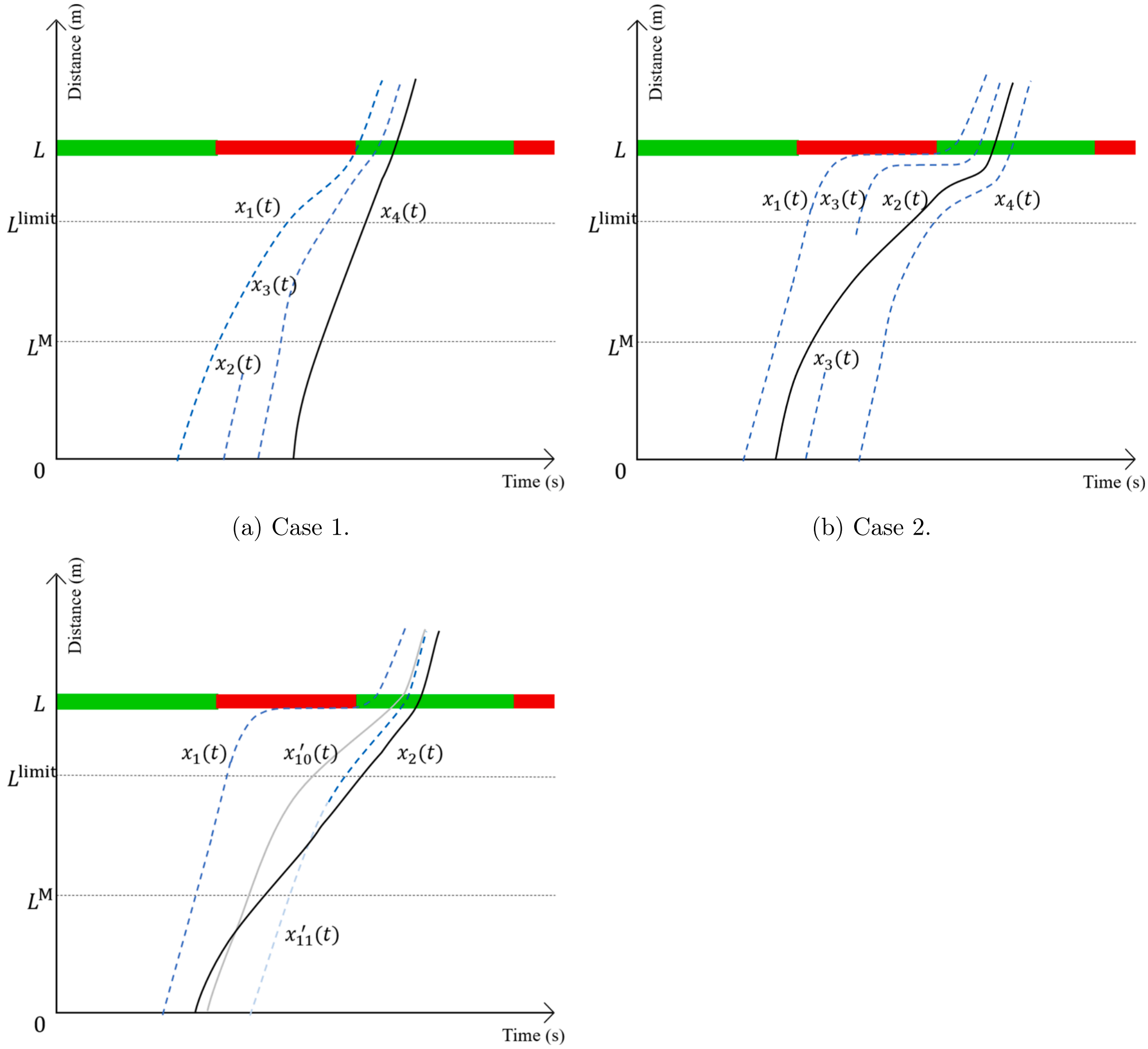

(a) Case 1. (b) Case 2.

(c) Case 3.

Fig. 15. Examples of three possible LC cases in LCTO.

and possible future directions to implement LCTO in real world.

As shown in Figs. 9, there exist some LCs in LCTO. Fig. 15 plots examples of three possible cases of LCs in LCTO. First, Case 1 shows a type of LCs that are not induced by TO. In Case 1, the blue-dashed curves denote the trajectories of HVs in the current lane (i.e., Vehicle 1, 2, and 3) and the black-solid curves denote the trajectories of CAVs in the current lane (i.e., Vehicle 4). Before CAV 4 arrives the control zone (i.e., Location 0), HV 2 changes its lane due to a low speed of HV 1 and a large spacing gap in the adjacent lane. Thus, CAV 4 does not have an opportunity to restrain this type of LCs. And we find that this type of LCs occurs more frequently at a low traffic saturation rate, as shown by those trajectories during the dissipation periods in Figs. 9 and 18. Second, Case 2 shows a second type of LCs that occur after a CAV. In Case 2, the blue-dashed curves denote the trajectories of HVs (i.e., Vehicles 1, 3, and 4), and the black-solid curves denote the trajectories of CAVs (i.e., Vehicle 2). When doing LCTO for CAV 2, HV 3 is considered as a following vehicle of CAV 2 in the same lane. Consequently, HV 3 changes its lane due to a low speed of CAV 2 and a large spacing gap in the adjacent lane, and then changes its lane in front of CAV 2 due to its mandatory lane changing behavior. The second type of LCs usually occurs at the beginning of a vehicle platoon. Finally, Case 3 shows a third type of LCs that are caused by the following CAVs in adjacent lanes. In Case 3, blue-dashed curves denote the trajectories of HVs in the current lane (i.e., Vehicle 1) and black-solid curves denote the trajectories of CAVs in the current lane (i.e., Vehicle 2). The light-blue-dashed curves denote the trajectories of HVs in the adjacent lane (i.e., Vehicle

11) and the grey-solid curves denote the trajectories of CAVs in the adjacent lane (i.e., Vehicle 10). In LCTO, the predefined car following models are used to predict trajectories of other vehicles. CAV 2 does not predict any LCs in adjacent lanes and thus plans its trajectory with a smoother trajectory. After that, CAV 10 arrives and plans its trajectory with LCTO, and then HV 11 changes lane in front of CAV 2 due to a low speed of CAV 10 and a large spacing gap in the adjacent lane. The third type of LCs occurs more frequently in a low traffic saturation rate, as shown by the trajectories during the dissipation periods in Figs. 9 and 18. Although the above analyses imply that LCTO has a limited lane-change-aware mechanism (i.e., the assumption of recognizing mandatory LCs as discretionary LCs if vehicles are unconnected and the simplifications of the LC-aware constraints to restrain all discretionary LCs), the results in the numerical experiments show that LCTO can still significantly improve the system performances by restraining most LCs. To address the recognition limitation, we can identify the mandatory LCs based on the behavior of a mandatory lane change vehicle that it will be persistent in making lane changes. For example, if we block a HV the first time and it keeps trying with upstream vehicles, we will identify it as a mandatory-LC vehicle. To address the limitation of simplification, an effective way might be using the reinforcement learning methods (e.g., Q-learning and the policy gradient algorithms) to build this problem as a Markov decision process considering a cooperative longitudinal and lateral trajectory planning mechanism. The goal of the reinforcement learning methods is to learn a policy that maximizes the expected return (e.g., throughput, fuel efficiency and safety) from the current state.

Additionally, we believe that LCTO can be extended from an isolated signalized intersection to a more complex geometric with multiple signalized intersections (e.g., signalized corridors). For controlling a signalized corridor, departed vehicles might need to be controlled as well. In this case, depending on the distance between two adjacent intersections and the road segment lengths, departed vehicles of one intersection might simply be seen as arrival vehicles by another intersection. This way, the proposed algorithm would be adaptable to handle a signalized corridor.

Further, this study assumes a fixed signal setting at intersections due to wide and simple implementations of fixed signal settings in real world. To extend LCTO from a fixed signal setting to an adaptive signal control (Feng et al., 2015), we can use a bi-level collaborative control framework that focuses the high-level signal control/optimization on a central controller while distributing complex low-level trajectory control to individual CAVs. This way, the extend collaborative control framework can further improve the system performance and easily be implemented in real world.

Finally, there exist a number of cyber-physical constraints in real-world applications. 1) This study assumes all CAVs are in the same cooperation class (cooperation class B or above defined by SAE J3216), however CAVs might have different cooperation classes in real world due to different designs of manufactures and preferences of riders. Thus, a mixed CAV cooperation class model needs to be extended from a mixed traffic with two types of vehicles (e.g., CAVs in the same cooperation class and HVs) to a mixed traffic with five types of vehicles (e.g., cooperation classes A-D CAVs and HVs). 2) This study assumes that all CAVs will accept the planned trajectories. Note that cooperation class C equipped CAVs have abilities to negotiate with other vehicles and accept/reject the planned trajectories. Thus, we need to use the game theory to decide the best strategy for accepting/rejecting the planned trajectories. 3) This study assumes that communication delays, sensing errors and prediction errors are neglected. Actually each vehicle may need to frequently (e.g., every 20 ms) adjust its direct drive-by-wire control variables (e.g., throttle and brake levels and steering wheel angle) to ensure the actual vehicle trajectory can closely follow the planned trajectory based on feedback controllers (e.g., the Model Predictive Control [MPC] and the proportional-integral-derivative [PID] controllers). An objective measure of the error will be proposed in the MPC (e.g., the weighted mean square errors of location and speed). In the PID control, each control variable is a simple linear function of the discrepancies of the status (e.g., locations and speeds) between the actual and the planned trajectories. Then, in the real-time control, a series of control variables will be optimized to minimize the expected objective error.

Overall, the proposed methodology in this study can be extended in number of ways as briefly illustrated above to deal with more complex real-world applications. This study plays an instrumental role and draws fundamental insights into studies focusing on trajectory smoothing with a lane-change-aware mechanism along signalized intersections with multi-lane roads.

6. Conclusion

This paper designs a mixed traffic framework at a signalized intersection with multi-lane roads including trajectory control, car following and lane changing maneuvers all together. HV LCs occur frequently due to lager gaps induced by CAV trajectory optimization and they may impair the expected system performance of the CAV trajectory optimization. To address this issue, this paper proposes a decentralized lane-change-aware CAV trajectory optimization model under the proposed framework considering a joint objective of riding comfort and mobility. Nonlinear lane-change-aware constraints including mandatory LC yielding and discretionary LC restraining strategies are linearized based on the solution in TO. After linearization, the proposed problem is converted to a quadratic optimization problem and can be solved easily by utilizing commercial solvers (e.g., Gurobi). Numerical experiments first investigate the system performance in CF, TO, LCTOY and LCTO at a signalized intersection with multi-lane roads. The results of CAV market penetration analyses show that the expected benefits of trajectory smoothing without considering LCs are decreased half or more due to HV LCs in TO. The results show that LCTO outperforms the other models. Especially, compared to TO, LCTO yields extra benefits in the system joint objective (about 10–25%), riding comfort (about 10–25%), travel time (about 1–8%), fuel consumption (about 3–15%) and safety (about 5–25%) when the CAV MPR is not extremely high. Sensitivity analysis results considering road segment lengths, signal cycle lengths, traffic saturation rates and through-vehicle rates show that LCTO has significant effects on restraining LCs induced by TO without being aware of possible LCs, and thus yields extra benefits in most traffic scenarios, such as 10–20% extra benefits when the road segment length is not extremely long, 15–30% extra benefits when the signal cycle length varies from 40 s to 120 s, 10%-25% extra benefits when the traffic saturation rate varies from 0.6 to 1.6, and 10–25% extra benefit when the through-vehicle rate is not extremely low.

This study reveals a significant potential of using a lane-change-aware mechanism in CAV trajectory smoothing concepts at a signalized intersection with multi-lane roads in transportation engineering applications. The study can be further extended in multiple directions. 1) Although using the proposed lane-change-aware trajectory optimization can improve the system performance, the lane-change-aware mechanism may not restrain all redundant LCs. To yield further benefits, reinforcement learning methods considering a cooperative longitudinal and lateral trajectory planning might be helpful. 2) This study is limited at an isolated signalized intersection. More complex geometric, such as corridors and networks, may be investigated in the future. 3) This study only considers a fixed signal setting. For variable signals, a cooperative optimization of signal timing and CAV trajectories may be developed to further improve the system performance. For an unsignalized intersection, a similar cooperative optimization of vehicle departure sequence and CAV trajectories could be implemented. 4) In real-time applications, the proposed method might suffer from certain cyber-physical constraints, such as mixed CAV cooperation classes, non-compliant behavior due to riders' preferences, communication delays, sensing errors, and prediction errors due to stochastic human driving behavior. Machine learning-based methods (e.g., long short-term memory neural networks, Gaussian process and deep deterministic policy gradient algorithm) could be implemented for trajectory prediction and trajectory planning (Zhou et al., 2020; Guo et al., 2021). Feedback controllers (e.g., MPC and PID controllers) could be developed to regulate CAV trajectories such that they will follow the planned trajectories when approaching to intersections. Such control strategies may address the implementation of trajectory smoothing concept in the real world and reduce the gaps between the actual system performance and theoretical system performance.

CRediT authorship contribution statement

Handong Yao: Conceptualization, Methodology, Software, Validation, Formal analysis, Visualization, Writing - original draft. **Xiaopeng Li**: Supervision, Conceptualization, Methodology, Formal analysis, Writing - reviewing & editing.

Acknowledgment

This research is supported by the U.S. National Science Foundation through Grants CMMI #1558887 and CMMI #1932452.

Appendix A. Notation List

Notation list.

Notation	Definition
$\mathcal{N} := [1, 2, \dots, N]$	Set of vehicles, where the number of vehicles is N.
$\mathcal{N}^{\mathrm{CAV}} := [1, 2, \dots, N^{\mathrm{CAV}}]$	Set of CAVs, where the number of CAVs is N^{CAV}.
$\mathcal{N}^{\mathrm{HV}} := [1, 2, \dots, N^{\mathrm{HV}}]$	Set of HVs, where the number of HVs is N^{HV}.
MPR	Market penetration rate, and MPR $= N^{\mathrm{CAV}}/N$.
$\mathcal{N}'$	Set of leading vehicles.
k	Index of lane $k \in \mathcal{K} := [1, K]$, where K is the number of lanes.
t	Index of time $t \in \mathcal{T} := [0, T]$, where T is the maximum simulation time.
n	Index of a vehicle, $n \in \mathcal{N}$.
l^{veh}	Length of a vehicle.
s_0^{CAV}	Minimum spacing of a CAV.
s_0^{HV}	Minimum spacing of an HV.
τ^{CAV}	Minimum time gap of a CAV.
τ^{HV}	Minimum time gap of an HV.
L	Location of stop-line, i.e., road segment length.
L^{limit}	Location of forbidding LCs.
L^{M}	Location of allowing mandatory LCs.
$\mathcal{X} := \{X_n\}_{n\in\mathcal{N}}$	Set of vehicle trajectories.
$X_n = \{x_n(t)\}_{t\in\mathcal{T}}$	Trajectory of vehicle $n \in \mathcal{N}$.
$x_n(t)$	Location of vehicle $n \in \mathcal{N}$ at time $t \in [0, T]$.
t_n^-	Time point of vehicle $n \in \mathcal{N}$ at location 0, i.e., arrival time.
t_n^+	Time point of vehicle $n \in \mathcal{N}$ at location L, i.e., departure time.
$v_n(t)$	Speed of vehicle $n \in \mathcal{N}$ at time $t \in [0, T]$, and $v_n(t) = \dot{x}_n(t)$.
$\overline{v}$	Speed limit (i.e., maximum allowed speed).
$a_n(t)$	Acceleration of vehicle $n \in \mathcal{N}$ at time $t \in [0, T]$, and $a_n(t) = \ddot{x}_n(t)$.
$\overline{a}$	Maximum acceleration.

(*continued on next page*)

(*continued*)

Notation	Definition
$\underline{a}$	Minimum acceleration (or maximum deceleration with a negative sign).
Δa	Changing threshold.
$o_n(t)$	Current lane of vehicle $n \in \mathcal{N}$ at time $t \in [0, T]$.
$o_n^*(t)$	Target lane of vehicle $n \in \mathcal{N}$ at time $t \in [0, T]$.
e_n	Desired movement of vehicle $n \in \mathcal{N}$.
$\widetilde{O}_n$	Desired lane set of vehicle $n \in \mathcal{N}$.
f^s	Traffic saturation rate.
G	Effective green length.
R	Effective red length.
C	Cycle length, and $C = G + R$.

Appendix B. Discrete models

Let $\mathcal{I} := [0, 1, 2, \ldots, I]$ denote the set of discrete-time points with a discrete-time interval Δt and a maximum discrete-time $I = \lceil T/\Delta t \rceil$. Let $i \in \mathcal{I}$ denote the index of a discrete-time point. Let $i_n^- := \lceil t_n^-/\Delta t \rceil$ denote the discretized arrival time of vehicle $n \in \mathcal{N}$. Let $i_n^+ := \lceil t_n^+/\Delta t \rceil$ denote the discretized departure time of vehicle n. Let $x_n[i]$, $v_n[i]$ and $a_n[i]$ denote the location, speed and acceleration of vehicle n at discrete-time point i, respectively. We also have $x_n[i] = x_n[i_n^-] + \sum_{j=i_n^-+1}^{i} v_n[j]\Delta t$, where $x_n[i_n^-] = v_n^- \times (i_n^-\Delta t - t_n^-)$ and $\overline{i_n^+} = \lceil \overline{t_n^+}/\Delta t \rceil$. Let $\mathcal{V}^{\mathrm{I}} := \{V_n^{\mathrm{I}}\}$ denote the set of discretized speeds, where $V_n^{\mathrm{I}} = \{v_n[i]\}_{i\in\mathcal{I}}$ is a sequence of vehicle n's discretized speeds.

For CAV $n \in \mathcal{N}^{\mathrm{CAV}}$, the discrete LCTO is then formulated as follows,

$$\text{DLCTO}: \min_{V_n^{\mathrm{I}}} J_n\left(V_n^{\mathrm{I}}\right) := \omega_m\left(L - x_n\left[\underline{i_n^+}\right]\right) + \omega_a \sum_{i=i_n^-}^{\overline{i_n^+}} \left(\frac{v_n[i+1] - v_n[i]}{\Delta t}\right)^2 \Delta t, \tag{36}$$

where $x_n\left[\underline{i_n^+}\right] = x_n\left[i_n^-\right] + \sum_{j=i_n^-+1}^{\underline{i_n^+}} v_n\left[j\right]\Delta t$ and $\underline{i_n^+} = \lceil \underline{t_n^+}/\Delta t \rceil$. If $L - x_n\left[\underline{i_n^+}\right]$ becomes smaller, the departure time t_n^+ will be closer to the $\underline{i_n^+}$ and thus it will decrease the travel time of CAV n. Further, the discrete LCTO is subject to

- Arrival constraint:

$$v_n\left[i_n^-\right] = v_n^-. \tag{37}$$

- Departure constraints:

$$L \leqslant x_n\left[\overline{i_n^+}\right] = x_n\left[i_n^-\right] + \sum_{j=i_n^-+1}^{\overline{i_n^+}} v_n\left[j\right]\Delta t \leqslant L + \overline{v} \times \left(\overline{\mathrm{i}_\mathrm{n}^+}\Delta \mathrm{t} - \overline{\mathrm{t}_\mathrm{n}^+}\right). \tag{38}$$

$$x_n\left[\underline{i_n^+}\right] = x_n\left[i_n^-\right] + \sum_{j=i_n^-+1}^{\underline{i_n^+}} v_n\left[j\right]\Delta t \leqslant L, \tag{39}$$

- Speed constraints:

$$0 \leqslant v_n\left[i\right] \leqslant \overline{v},\ \forall i \in \left[i_n^-, \overline{i_n^+}\right]. \tag{40}$$

- Acceleration constraints:

$$\underline{a} \leqslant a_n\left[i\right] = \frac{v_n[i+1] - v_n[i]}{\Delta t} \leqslant \overline{a},\ \forall i \in \left[i_n^-, \overline{i_n^+}\right]. \tag{41}$$

- Safety constraints:

$$x_{l_n[i_n^-]}\left[i\right] - x_n\left[i\right] = x_{l_n[i_n^-]}\left[i\right] - \left(x_n\left[i_n^-\right] + \sum_{j=i_n^-+1}^{i} v_n\left[j\right]\Delta t\right) \geqslant s_0^{\mathrm{CAV}} + l^{\mathrm{veh}} + v_n\left[i\right]\tau^{\mathrm{CAV}}, \forall i \in \left[i_n^-, \overline{i_n^+}\right], \tag{42}$$

- LC-aware constraints:

$$\left(1-\beta_{p_n[i]}\left[i\right]\right)\times\left(x_{p_n[i]}\left[i\right]-x_n\left[i\right]-\left(s_0^{\mathrm{CAV}}+l^{\mathrm{veh}}\right)-\tau^{\mathrm{CAV}}v_n\left[i\right]\right)\le 0,\ \forall i\in\left[\underline{i_n^-},\overline{i_n^+}\right]. \tag{43}$$

$$\beta_{p_n[i]}\left[\left[i\right]\right]=\left\{0,\quad \text{if } \widetilde{a}_{p_n[i],\widehat{l}_{p_n[i]}[i]}\left[i\right]-\widetilde{a}_{p_n[i],l_{p_n[i]}[i]}\left[i\right]>0.1 \quad \text{or } s_{p_n[i],\widehat{l}_{p_n[i]}[i]}\left[i\right]>s_0^{\mathrm{HV}}+\tau^{\mathrm{HV}}v_{p_n[i]}\left[i\right], 1, \text{otherwise}.\right. \tag{44}$$

Eq. (38) then is reformulated as a general linear function

$$A_0\left[i\right]+A_1\left[i\right]x_n\left[\underline{i_n^-}\right]+A_1\left[i\right]\Delta t\sum_{j=\underline{i_n^-}+1}^{i}v_n\left[j\right]+A_2\left[i\right]v_n\left[i\right]\le 0,\forall i\in\left[\underline{i_n^-},\overline{i_n^+}\right], \tag{45}$$

where $A_0[i]=(1-\beta_{p_n[i]}[i])\times(x_{p_n[i]}[i]-(s_0^{\mathrm{CAV}}+l^{\mathrm{veh}}))$, $A_1[i]=-(1-\beta_{p_n[i]}[i])$, and $A_2[i]=(1-\beta_{p_n[i]}[i])\times(-\tau^{\mathrm{CAV}})$.

To be compared with the discrete LCTO, a discrete TO is also formulated for CAV $n\in\mathcal{N}^{\mathrm{CAV}}$,

$$\mathrm{DTO}:\ \min_{V_n^{\mathrm{I}}}J_n\left(V_n^{\mathrm{I}}\right):=\sum_{n=1}^{N}\left(\omega_m\left(L-x_n\left[\underline{i_n^+}\right]\right)+\omega_a\sum_{i=\underline{i_n^-}}^{\overline{i_n^+}}\left(\frac{v_n[i+1]-v_n[i]}{\Delta t}\right)^2\Delta t\right), \tag{46}$$

subject to Eqs. (37)–(42).

Appendix C. Selection of weights

To select suitable weights of mobility and riding comfort (i.e., squared acceleration), we compare LCTO with CF by setting the weight of squared acceleration $\omega_a=1$ and varying the weight of mobility $\omega_m\in[0,2]$ with an increment of 0.1. The result is shown in Fig. 16. The black-solid curve depicts the benefit of the system riding comfort in LCTO. The red-dashed curve depicts the benefit of the system travel time in LCTO. We find that the benefit of the system riding comfort decreases in a small range (from 94% to 91%) as the weight of mobility grows, and it becomes stable when $\omega_m\ge 0.5$. Additionally, the benefit of the system travel time increases as the weight of mobility grows. When $\omega_m\le 0.2$, LCTO focuses more on the system riding comfort and it may sacrifice the system travel time to increase the system riding comfort. Thus, the benefit of the system travel time is negative. We also find that the benefit of the system travel time becomes stable when $\omega_m\ge 1$. Therefore, we select $\omega_m=1$ to ensure positive and stable benefits of the system riding comfort and travel time. After the selection of weights, we will conduct a set of numerical experiments to investigate the performance of TO and LCTO.

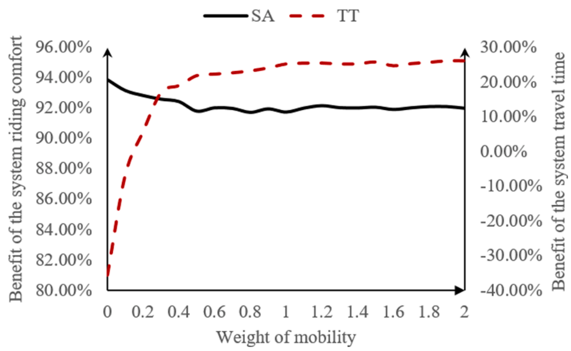

Fig. 16. Selection of weights.

Appendix D. Extension with three-or-more roads

From the above analyses, we find that LCTO yields more benefits than TO at a signalized intersection with two-lane roads. To generalize LCTO at a signalized intersection with three-or-more-lane roads, we extend the lane changing model and conduct another set of experiments.

Assume a multi-lane road with K lanes, as shown in Fig. 17. HV n is the subject vehicle, and vehicle l_n is HV n's preceding vehicle in the same lane. $\widehat{l}_n^R$ and $\widehat{l}_n^L$ denote HV n's preceding vehicles in right and left adjacent lanes, respectively. $\widehat{f}_n^R$ and $\widehat{f}_n^L$ denote HV n's following vehicles in right and left adjacent lanes, respectively. Assign lane 1 to left-turn vehicles only and lane K to right-turn vehicles only. Thus, the desired lane set $\widetilde{O}_n(e_n)$ of vehicle n is formulated as follows,

$$\widetilde{O}_n(e_n) = \begin{cases} \{2, \ldots, K\}, & \text{if } e_n = 0; \\ \{1\}, & \text{if } e_n = 1; \\ \{K\}, & \text{otherwise.} \end{cases} \tag{47}$$

Thus, the vehicles in the leftmost and rightmost lanes follow the Eqs. (21)–(20). The other vehicles in the middle lanes need to consider both adjacent lanes. Then, we need to find the target lane that HV n desires to change lane to. For discretionary LC vehicles (i.e., $\widetilde{o}_n = 0$), the incentive check (i.e., Eq. (21)) is reformulated as follows,

$$\max\left\{\widetilde{a}_{n,\widehat{l}_n^R(t)}\left(t\right), \widetilde{a}_{n,\widehat{l}_n^L(t)}\left(t\right)\right\} - \widetilde{a}_{n,l_n(t)}\left(t\right) > \Delta a_n(t). \tag{48}$$

The preceding vehicle $\widehat{l}_n^*(t)$ in the target lane $o_n^*(t)$ is obtained by

$$\widehat{l}_n^*\left(t\right) = \left\{ \widehat{l}_n^R\left(t\right), \text{if } \widetilde{a}_{n,\widehat{l}_n^R(t)}\left(t\right) > \widetilde{a}_{n,\widehat{l}_n^L(t)}\left(t\right), \widehat{l}_n^L\left(t\right), \text{otherwise.} \right. \tag{49}$$

$$o_n^*\left(t\right) = \left\{ \min\{o_n(t)+1, K\}, \quad \text{if } \widetilde{a}_{n,\widehat{l}_n^R(t)}\left(t\right) > \widetilde{a}_{n,\widehat{l}_n^L(t)}\left(t\right), \max\{o_n(t)-1, 1\}, \text{otherwise.} \right. \tag{50}$$

Then, the target lane $\widehat{l}_n^*(t)$ is used to replace $\widehat{l}_n(t)$ in safety checks (i.e., Eqs. (19) and (20)).

With the above equations, we can study the lane changing behavior at a signalized intersection with three-or-more-lane roads. We will study a signalized intersection with 3, 4, and 5 lanes under different CAV MPRs, respectively. MPR_k in each lane is set from 10% to 100% with an increment of 10%, and these values in all lanes will vary simultaneously. The other parameters are set at their default values as in Section 4.2.

Fig. 18 shows examples of trajectories in TO and LCTO at a signalized intersection with three-lane roads under 50% CAV MPR. We find that a number of HV LCs occur in TO, and thus it causes "stop-and-go" traffic and "spillback" traffic. However, there are less LCs in LCTO, and it causes less "stop-and-go" traffic and no "spillback" traffic. Also, we find that an HV changes its lane from lane 2 to lane 1 and then becomes the first vehicle in lane 1 due to LCTO in Fig. 18 (b). This shows that LCTO will yield to mandatory LCs but there is no such mechanism in TO. Therefore, the results verify the effectiveness of LCTO at a signalized intersection with three-lane roads.

Further, Fig. 19 plots the performance of LCTO with varying CAV MPRs at a signalized intersection with two-lane, three-lane, four-

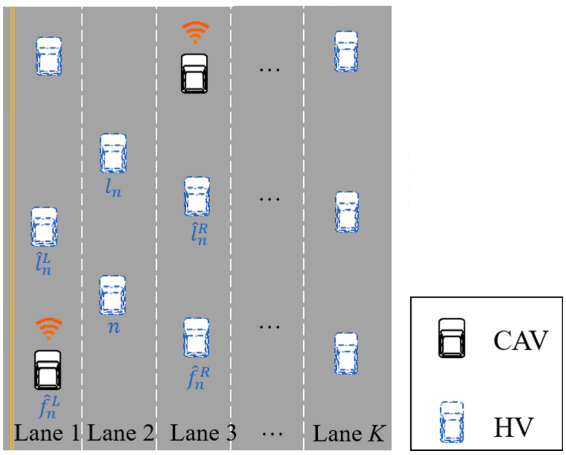

Fig. 17. An Illustration of LCs in a multi-lane road.

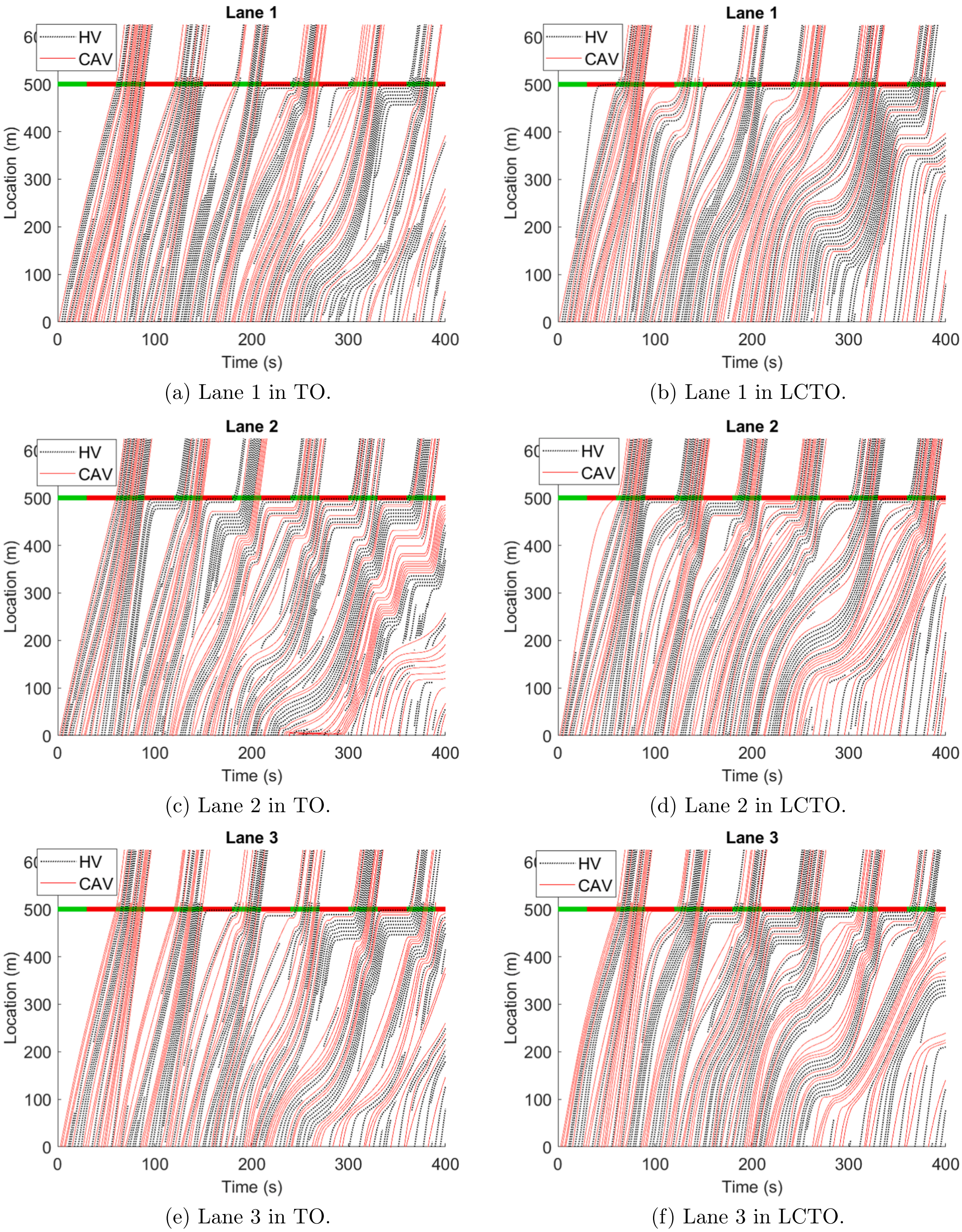

Fig. 18. Examples of trajectory results in TO and LCTO at a signalized intersection with three-lane roads.

lane and five-lane roads, respectively. The black-solid curve, the red-dashed curve, the green-dash-dotted curve, and the gray-dotted curve denote the benefits with 2-lane, 3-lane, 4-lane, and 5-lane settings, respectively. Fig. 19 (a) shows the benefits of the system joint objective in LCTO compared with those in CF. Since more LCs occur as the lane number increases, the benefit of LCTO decreases. From Fig. 19 (b), we find that the extra benefits in the three-or-more-lane experiments have a similar trend (i.e., increases initially and then decreases with the increasing CAV MPR) as in the two-lane experiments. However, more extra benefits of LCTO are found with more lanes at high CAV MPRs. This is probably because that there are more HVs and more opportunities for making LCs in the experiments

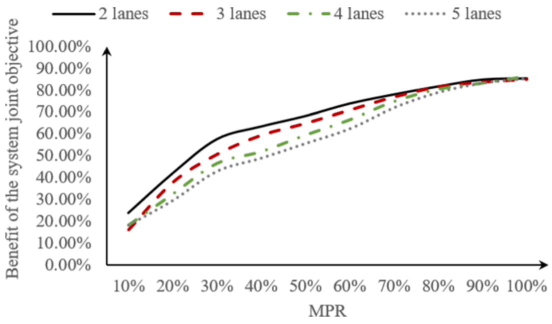

(a) LCTO - CF.

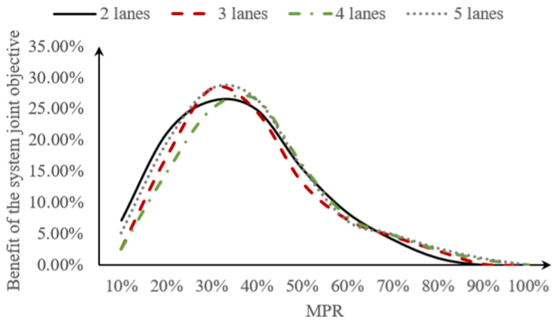

(b) LCTO-TO.

Fig. 19. The system performance of LCTO with varying CAV MPRs at a signalized intersection with multi-lane roads.

with more lanes. Overall, LCTO is capable to restrain LCs and improve the system performance at a signalized intersection with three-or-more-lane roads.

Appendix E. Impacts of stochastic HV car following behavior

In reality, the trajectories of HVs might not be predicted accurately with a deterministic car following model due to the stochasticity of HV car following behavior. Thus, we add a White Gaussian noise with mean 0 and variance σ^2 (i.e., $W \backsim N(0,\sigma^2)$) into the deterministic car following model (Laval et al., 2014) to represent the stochasticity of HV car following behavior. The actual acceleration with stochasticity is reformulated as follows,

$$a_n^s\left(t\right) = \max\left(\underline{a}, \min(\overline{a}, a_n(t) + W)\right), \tag{51}$$

where $a_n(t)$ is calculated based on the deterministic Gipps' car following model (i.e., Eqs. 17 and 18). The probability density function of W is

$$f_W(w) = \frac{1}{\sigma\sqrt{2\pi}} e^{\frac{-w^2}{2\sigma^2}}, \tag{52}$$

Then, we vary σ between 0 and 1 m/s^2 with an increment of 0.2 m/s^2 while fixing the other parameters at their default values. The preliminary results are shown in Fig. 20. As σ grows, the error between the actual and predicted acceleration becomes greater. Such error will cause "stop-and-go" traffic that is not considered by the planned trajectory. Thus, the performance of both LCTO and TO will be impaired as σ grows. Further, we find that LCTO could yield significant extra benefit (15–30%) compared with TO even when considering the stochastic car following behavior. In the future, we will use machine learning-based methods (e.g., LSTM and Gaussian process) to predict the stochastic HV car following behavior. And then CAV trajectories will be planned and controlled based on the prediction of the stochastic HV car following behavior.

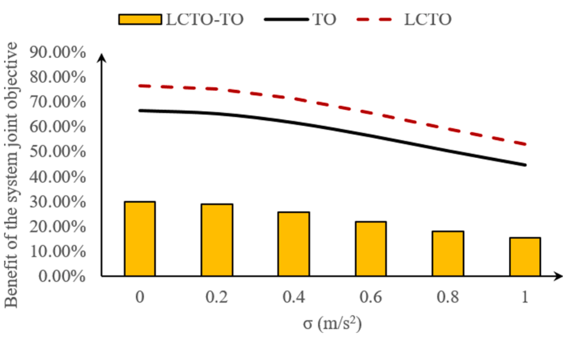

Fig. 20. The system performance of LCTO with the impacts of stochastic car following behavior.

References

Aria, E., Olstam, J., Schwietering, C., 2016. Investigation of Automated Vehicle Effects on Driver's Behavior and Traffic Performance. Transp. Res. Procedia 15, 761–770. https://doi.org/10.1016/j.trpro.2016.06.063.

Bevly, D., Cao, X., Gordon, M., Ozbilgin, G., Member, S., Kari, D., Nelson, B., Woodruff, J., Barth, M., Murray, C., Kurt, A., Redmill, K., Member, S., Ozguner, U., 2016. Lane Change and Merge Maneuvers for Connected and Automated Vehicles: A Survey. IEEE Trans. Intell. Veh. 1, 105–120. https://doi.org/10.1109/TIV.2015.2503342.

Chen, D., Ahn, S., Chitturi, M., Noyce, D.A., 2017. Towards vehicle automation: Roadway capacity formulation for traffic mixed with regular and automated vehicles 100, 196–221. doi: 10.1016/j.trb.2017.01.017.

Chen, N., Arem, B.V., Member, S., Alkim, T., Wang, M., 2020. A Hierarchical Model-Based Optimization Control Approach for Cooperative Merging by Connected Automated Vehicles, 1–14.

Choi, K., Gi, H., 2019. Cut-in vehicle warning system exploiting multiple rotational images of SVM cameras. Expert Syst. Appl. 125, 81–99. https://doi.org/10.1016/j.eswa.2019.01.081.

DOT, U.S., 2018. Preparing for the Future of Transportation: Automated Vehicles 3.0. US https://www.transportation.gov/av/3.

Feng, Y., Head, K.L., Khoshmagham, S., Zamanipour, M., 2015. A real-time adaptive signal control in a connected vehicle environment. Transp. Res. Part C 55, 460–473. https://doi.org/10.1016/j.trc.2015.01.007.

Gettman, D., Head, L., 1840. Surrogate Safety Measures from Traffic Simulation Models, pp. 104–115.

Ghiasi, A., Li, X., Ma, J., 2019. A mixed traffic speed harmonization model with connected autonomous vehicles. Transp. Res. Part C 104, 210–233. https://doi.org/10.1016/j.trc.2019.05.005.

Guo, Q., Angah, O., Liu, Z., Ban, X.J., 2021. Hybrid deep reinforcement learning based eco-driving for low-level connected and automated vehicles along signalized corridors. Transp. Res. Part C 124, 102980. https://doi.org/10.1016/j.trc.2021.102980.

He, X., Wu, X., 2018. Eco-driving advisory strategies for a platoon of mixed gasoline and electric vehicles in a connected vehicle system. Transp. Res. Part D 63, 907–922. https://doi.org/10.1016/j.trd.2018.07.014.

International, S.A.E., 2020. Taxonomy and Definitions for Terms Related to Cooperative Driving Automation for On-Road Motor Vehicles J3216_202005.

Ioannou, P.A., Stefanovic, M., Member, S., 2005. Evaluation of ACC Vehicles in Mixed Traffic: Lane Change Effects and Sensitivity Analysis 6, 79–89.

Jiang, H., Hu, J., An, S., Wang, M., Park, B.B., 2017. Eco approaching at an isolated signalized intersection under partially connected and automated vehicles environment. Transp. Res. Part C: Emerg. Technol. 79, 290–307. https://doi.org/10.1016/j.trc.2017.04.001. https://linkinghub.elsevier.com/retrieve/pii/S0968090X17301067.

Kamal, M.A.S., Taguchi, S., Yoshimura, T., 2015. Intersection Vehicle Cooperative Eco-Driving in the Context of Partially Connected Vehicle Environment, 1261–1266. doi: 10.1109/ITSC.2015.207.

Kazemi, H., Mahjoub, H.N., Tahmasbi-sarvestani, A., Fallah, Y.P., 2018. A Learning-Based Stochastic MPC Design for Cooperative Adaptive Cruise Control to Handle Interfering Vehicles 3, 266–275.

Ko, W., Chang, D.E., 2018. Cooperative Adaptive Cruise Control Using Turn Signal for Smooth and Safe Cut-In, 807–812.

Laval, J.A., Toth, C.S., Zhou, Y., 2014. A parsimonious model for the formation of oscillations in car-following models. Transp. Res. Part B: Methodol. 70, 228–238. https://doi.org/10.1016/j.trb.2014.09.004.

Li, Q., Li, X., Mannering, F., 2021. Assessment of discretionary lane-changing decisions using a random parameters approach with heterogeneity in means and variances. Transp. Res. Rec. 0361198121992364.

Liu, H., David, X., Shladover, S.E., Lu, X.y., Ferlis, R.E., 2018. Modeling impacts of Cooperative Adaptive Cruise Control on mixed traffic flow in multi-lane freeway facilities. Transp. Res. Part C 95, 261–279. https://doi.org/10.1016/j.trc.2018.07.027.

Ma, J., Li, X., Zhou, F., Hu, J., Park, B.B., 2017. Parsimonious shooting heuristic for trajectory design of connected automated traffic part II: Computational issues and optimization. Transp. Res. Part B: Methodol. 95, 421–441. https://doi.org/10.1016/j.trb.2016.06.010.

Milanés, V., Shladover, S.E., 2016. Handling Cut-In Vehicles in Strings of Cooperative Adaptive Cruise Control Vehicles Handling Cut-In Vehicles in Strings of Cooperative Adaptive Cruise 2450. doi: 10.1080/15472450.2015.1016023.

Muslim, H., Itoh, M., 2018. Automation Interventions for Avoiding, 2711–2716. doi:10.1109/SMC.2018.00463.

Pourmehrab, M., Elefteriadou, L., Ranka, S., Martin-gasulla, M., 2020a. Optimizing Signalized Intersections Performance Under Conventional and Automated Vehicles Traffic 21, 2864–2873.

Pourmehrab, M., Emami, P., Martin-gasulla, M., Wilson, J., Elefteriadou, L., Ph, D., Ranka, S., Ph, D., 2020b. Signalized Intersection Performance with Automated and Conventional Vehicles: A Comparative Study 146, 1–9. doi:10.1061/JTEPBS.0000409.

Slade, P., Taylor, P., Chowdhury, F.R., Zhang, L., 2020. A mixed integer programming formulation and scalable solution algorithms for traffic control coordination across multiple intersections based on vehicle space-time trajectories. Transp. Res. Part B 134, 266–304. https://doi.org/10.1016/j.trb.2020.01.006.

Sun, W., Wang, Y., Yu, G., Liu, H.X., 2015. Quasi-optimal feedback control for a system of oversaturated intersections. Transp. Res. Part C 57, 224–240. https://doi.org/10.1016/j.trc.2015.06.018.

Taylor, P., Zhou, X., 2017. Recasting and optimizing intersection automation as a connected-and-automated-vehicle (CAV) scheduling problem: A sequential branch-and-bound search approach in phase-time-traffic hypernetwork. Transp. Res. Part B 105, 479–506. https://doi.org/10.1016/j.trb.2017.09.020.

Treiber, M., Kesting, A., 2013. Traffic Flow Dynamics. doi: 10.1007/978-3-642-32460-4.

Treiber, M., Kesting, A., Model, A.C.F., 2014. Automatic and efficient driving strategies while approaching a traffic light, 1122–1128.

Wan, N., Vahidi, A., Luckow, A., 2016. Optimal speed advisory for connected vehicles in arterial roads and the impact on mixed traffic q. Transp. Res. Part C 69, 548–563. https://doi.org/10.1016/j.trc.2016.01.011.

Wang, M., Hoogendoorn, S.P., Daamen, W., Arem, B.V., Happee, R., 2015. Game theoretic approach for predictive lane-changing and car-following control. Transp. Res. Part C 58, 73–92. https://doi.org/10.1016/j.trc.2015.07.009.

Wang, Y., Li, X., Yao, H., 2018. Review of trajectory optimisation for connected automated vehicles. doi: 10.1049/iet-its.2018.5184.

Wei, Y., Avci, C., Liu, J., Belezamo, B., Aydin, N., Li, P., Zhou, X., 2017. Dynamic programming-based multi-vehicle longitudinal trajectory optimization with simplified car following models. Transp. Res. Part B: Methodol. 106, 102–129. https://doi.org/10.1016/j.trb.2017.10.012. https://linkinghub.elsevier.com/retrieve/pii/S0191261517301078.

Xia, H., Boriboonsomsin, K., Barth, M., Xia, H., Boriboonsomsin, K., Barth, M., 2013. Dynamic Eco-Driving for Signalized Arterial Corridors and Its Indirect Network-Wide Energy/ Emissions Benefits Dynamic Eco-Driving for Signalized Arterial Corridors and Its Indirect Network-Wide Energy/ Emissions 2450. doi: 10.1080/15472450.2012.712494.

Yang, H., Rakha, H., Ala, M.V., 2017. Eco-Cooperative Adaptive Cruise Control at Signalized Intersections Considering. IEEE Trans. Intell. Transp. Syst. 18, 1575–1585. https://doi.org/10.1109/TITS.2016.2613740.

Yao, H., Li, X., 2020. Decentralized control of connected automated vehicle trajectories in mixed traffic at an isolated signalized intersection. Transp. Res. Part C 121, 102846.

You, F., Zhang, R., Lie, G., Wang, H., Wen, H., Xu, J., 2015. Expert Systems with Applications Trajectory planning and tracking control for autonomous lane change maneuver based on the cooperative vehicle infrastructure system. Expert Syst. Appl. 42, 5932–5946. https://doi.org/10.1016/j.eswa.2015.03.022.

Yu, C., Feng, Y., Liu, H.X., Ma, W., Yang, X., 2018. Integrated optimization of traffic signals and vehicle trajectories at isolated urban intersections. Transp. Res. Part B 112, 89–112. https://doi.org/10.1016/j.trb.2018.04.007.

Zegeye, S.K., Schutter, B.D., Hellendoorn, J., Breunesse, E.A., Hegyi, A., 2013. Integrated macroscopic traffic flow, emission, and fuel consumption model for control purposes. Transp. Res. Part C 31, 158–171. https://doi.org/10.1016/j.trc.2013.01.002.

Zhang, Y., Lin, Q., Wang, J., Verwer, S., Dolan, J.M., 2018. Lane-Change Intention Estimation for Car-Following Control in Autonomous Driving 3, 276–286.

Zhao, W., Ngoduy, D., Shepherd, S., Liu, R., Papageorgiou, M., 2018. A platoon based cooperative eco-driving model for mixed automated and human-driven vehicles at a signalised intersection. Transp. Res. Part C: Emerg. Technol. 95, 802–821. https://doi.org/10.1016/j.trc.2018.05.025. URL: https://linkinghub.elsevier.com/retrieve/pii/S0968090X18307423.

Zhou, M., Yu, Y., Qu, X., 2020. Development of an Efficient Driving Strategy for Connected and Automated Vehicles at Signalized Intersections: A Reinforcement. IEEE Trans. Intell. Transp. Syst. 21, 433–443. https://doi.org/10.1109/TITS.2019.2942014.